Maximum-entropy principle for ac and dc dynamic high-field transport in monolayer graphene (F)

M. Trovato, P. Falsaperla (iD), and L. Reggiani

COLLECTIONS

(F) This paper was selected as Featured

View Online   Export Citation   CrossMark

ARTICLES YOU MAY BE INTERESTED IN

Maximum-entropy principle for ac and dc dynamic high-field transport in monolayer graphene (F)

M. Trovato,[1,a] P. Falsaperla,[1,b] (iD) and L. Reggiani[2,c]

AFFILIATIONS

[1]Dipartimento di Matematica, Università di Catania, Viale A. Doria, 95125 Catania, Italy
[2]Dipartimento di Matematica e Fisica, "Ennio de Giorgi," Università del Salento, via Monteroni, I-73100 Lecce, Italy

[a]trovato@dmi.unict.it
[b]falsaperla@dmi.unict.it
[c]lino.reggiani@unisalento.it

ABSTRACT

Using the maximum entropy principle, we present a general theory to describe ac and dc high-field transport in monolayer graphene within a dynamical context. Accordingly, we construct a closed set of hydrodynamic (HD) equations containing the same scattering mechanisms used in standard Monte Carlo (MC) approaches. The effects imputable to a linear band structure, the role of conductivity effective mass of carriers, and their connection with the coupling between the driving field and the dissipation phenomena are analyzed both qualitatively and quantitatively for different electron densities. The theoretical approach is validated by comparing HD results with existing MC simulations.

Published under license by AIP Publishing. https://doi.org/10.1063/1.5088809

I. INTRODUCTION

In the last few decades, the maximum entropy principle (MEP)[1–3] emerged as a powerful method to develop rigorous hydrodynamic (HD) models both in classic[3–6] and in quantum[3,7–9] statistical mechanics. In particular, by starting from microscopic dynamics (band structure and scattering mechanisms), the MEP managed to provide physical insight into the origin of different terms entering the HD equations, thus leading to a renewed interest in the construction of self-consistent closure relations to investigate charge transport in semiconductors.[3,10–14]

The aim of this work is to develop and apply a general theory of MEP to analyze high-field transport in monolayer graphene. The theory is formulated at a kinetic level, without the need to introduce external parameters and the MEP is used in a local dynamic contest. The main objectives address three main interdisciplinary topics: statistical physics, nonlinear dynamics, and computational physics. Accordingly, we assert that the MEP is a fundamental postulate in statistical mechanics because it allows us to describe the thermodynamic evolution of a nonequilibrium system compatibly with the statistics, with the band structure, and with scattering mechanisms for any system of carriers in gas-dynamics and in solid-state physics, as in the case considered here of hot carriers in graphene.

In particular, we believe that the present formulation of MEP for Fermi 2D systems and its application to describe the transport properties of graphene advances significantly the state of knowledge existing in the literature, for the following reasons:

(i)   By using the MEP, we propose a systematic strategy to construct a new set of closed HD models (using an arbitrary number of moments) containing the underlying physical processes in an explicit way, i.e., the same band model and scattering mechanisms used in any other kinetic approach [for example, in Monte Carlo (MC) simulations].
(ii) The proposed HD systems are convergent, in correspondence with an increasing number of moments, and the final HD results compare very well with equivalent MC simulations.
(iii) From the point of view of computational physics, when compared with the MC method, the HD-MEP approach exhibits

the relevant advantage of requiring the same input data while significantly reducing the computational effort. As an example, for any single simulation under stationary conditions and for about 100 values of electric fields in the range [0; 80] kV/cm, also using a large number of moments, all the HD results are obtained with computational times shorter than 1 min on a standard workstation.

(iv) By using the present HD-MEP approach, within a small-signal analysis, the nature and the characteristics of the collisional processes can be easily investigated. The effects imputable to a linear band structure, the role of conductivity effective mass of carriers, and their connection with the coupling between the driving field and the dissipation phenomena are analyzed both qualitatively and quantitatively for different electron densities. In particular, we prove that the dissipative processes are substantially connected with the randomization of the group velocity and that the occurrence of a "negative differential mobility" (NDM) for the average velocity is, therefore, imputable to the combined action of the linear band structure, of the effective mass, of the external field, and of the scattering mechanisms.

The content of the paper is organized as follows. In Sec. II, we present the general theory for electron transport in monolayer graphene. To this purpose, we consider an arbitrary number of moments of the distribution function using a linear approximation of the MEP and we construct the corresponding closed HD system of equations. Here, we explain the effects due to a linear band structure considering its connection with both the conductivity effective mass and the electrons' group velocity. Besides, the theory of small-signal response under space-homogenous conditions is developed. In Sec. III, we analyze the collisional frequencies for different electron densities and different ranges of electric fields. We discuss the numerical convergence of the HD approach. By keeping unchanged the modulus of the group velocity, we show that the external field and the scattering processes can only align or randomize its direction with respect to the applied field. Here, we prove that the alternation and the competition between these processes, together with the effects of linear band structure, can lead to the onset of an NDM for the average velocity. In particular, for very low electric fields, we show that the number of collisional events is strongly dependent on the electron density, and, as a consequence, the behavior of the NDM will depend strongly on the carrier density. Finally, within a small-signal analysis, the nature and the characteristics of the collisional processes are investigated. In this way, we prove that for any electron density, a streaming motion regime[15] is obtained in a range of electric fields much wider than in the case of standard semiconductors.[3,14–16] A detailed comparison of present calculations with existing MC simulations is then carried out. The overall agreement is used to validate the theoretical approach and to provide a systematic physical insight into the microscopic dynamics. Major conclusions are given in Sec. IV. Finally, the derivation of some analytical results is summarized in Appendixes A–C. In particular, the connections between the conductivity effective mass and the introduction of a Lorentz factor for the system, and, more generally, the analogies between the monolayer graphene and other physical systems in which we have a saturation velocity for the charge carriers are explicitly explained in Appendixes A–C.

II. GENERAL THEORY

In graphene, carriers can be described by taking an analytic approximation for the band structure near the Dirac points.[17] In particular, for both the conduction band ($\pi^\star$ band) and the valence band (π band), we can consider two equivalent valleys (**K** and **K′** valleys) with an energy dispersion described by a linear relation $\varepsilon(\vec{k}) = \pm \hbar v_F k$, with $\hbar$ being the reduced Planck constant, $v_F \approx 10^6$ m/s the Fermi velocity, $\vec{k}$ the wavevector, with the $\pm$ signs referring to conduction and valence bands, respectively.[17] To describe a simplified carrier dynamics, we assume a concentration of electrons in the conduction band sufficiently high to justify the neglect of the hole dynamics. In the framework of a kinetic theory, this implies that the carrier system will be described by considering only the distribution function of electrons in the conduction band.

A. Kinetic approach and scattering rates

Following the previous approximations, we can treat (i) the two equivalent **K** and **K′** valleys of the $\pi^\star$ band as one effective valley, with the linear band structure $\varepsilon(\vec{k}) = \hbar v_F k$, (ii) all interband transitions are neglected, (iii) the main scattering processes are only due to intraband electron-phonon interactions, which produce intervalley and intravalley transitions.

Using the results of density functional theory (DFT), for the inelastic transitions, we consider the intravalley scattering processes assisted by optical phonons (LO, TO)[17–20] and the $K-K'$ intervalley processes assisted by the combined contribution of LA and TA acoustic phonons.[19,20] In the compact form, we will refer to these inelastic scattering processes with the index $\eta = \{LO, TO, LA, TA\}$. For elastic (EL) transitions, we will consider the intravalley scattering with acoustic phonons by taking the longitudinal modes only.[17,21]

At a kinetic level, the microscopic description is governed by the Boltzmann transport equation (BTE) for the distribution function $\mathscr{F}(\vec{k}, \vec{r}, t)$,

$$\frac{\partial \mathscr{F}}{\partial t} + u_i \frac{\partial \mathscr{F}}{\partial x_i} - \frac{e}{\hbar} E_i \frac{\partial \mathscr{F}}{\partial k_i} = Q(\mathscr{F}), \qquad (1)$$

with $u_i(\vec{k}) = \hbar^{-1} \partial \varepsilon / \partial k_i = v_F k_i / k$ being the carrier group velocity, e the unit charge, E_i the electric field, and

$$Q(\mathscr{F}) = \sum_\eta Q_\eta(\mathscr{F}) + Q_{ac}^{EL}(\mathscr{F}) \qquad (2)$$

is the total collision operator, where Q_η and Q_{ac}^{El} are the collisional integrals for the relevant electron-phonon scattering processes in monolayer graphene.

In particular, for the different phonon modes η, it is $Q_\eta = \int d\vec{k'} S_\eta(\vec{k}, \vec{k'}) [\mathscr{F'}(1 - \mathscr{F}/y) - \mathscr{F}(1 - \mathscr{F'}/y)]$, where $\mathscr{F} = \mathscr{F}(\vec{k}, \vec{r}, t)$, $\mathscr{F'} = \mathscr{F}(\vec{k'}, \vec{r}, t)$, the constant $y = (2\tilde{s} + 1)/(2\pi)^2$ which takes into account the spin degeneration,[3] where $\tilde{s}\hbar$ is the particle spin, and

$$S_\eta(\vec{k}, \vec{k'}) = \frac{|\mathscr{D}_\eta(\vec{k}, \vec{k'})|^2}{4\pi \rho \omega_\eta} \begin{bmatrix} N_\eta \\ N_\eta + 1 \end{bmatrix} \delta[\varepsilon' - (\varepsilon \mp \hbar \omega_\eta)] \qquad (3)$$

is the inelastic scattering rate from state $\vec{k'}$ to state $\vec{k}$, with $\mathscr{D}_\eta(\vec{k}, \vec{k'})$

being the electron-phonon coupling (EPC) matrix elements, ρ the graphene density, ω_η the phonon angular frequency, $N_\eta = 1/[\exp(\hbar\omega_\eta/k_B T_0) - 1]$ the phonon occupation number (with T_0 being the lattice temperature and k_B the Boltzmann constant), $\varepsilon' = \varepsilon(\vec{k}')$ and $\varepsilon = \varepsilon(\vec{k})$, while the upper and the lower options in the expression correspond to absorption and emission, respectively.

The EPC matrix elements, for the inelastic intravalley processes assisted by phonons Γ_{Lo}, Γ_{To}, are given by[18]

$$| \mathscr{D}_\eta(\vec{k}, \vec{k}') |^2 = \begin{cases} D_\Gamma^2[1 - \cos(\theta'' + \theta')], & \eta = LO, \\ D_\Gamma^2[1 + \cos(\theta'' + \theta')], & \eta = TO, \end{cases} \quad (4)$$

where D_Γ is the empiric deformation potential, θ'' refers to the angle between $\vec{k}$ and $\vec{k}' - \vec{k}$, θ' describes the angle between $\vec{k}'$ and $\vec{k}' - \vec{k}$. Thus, by calculating the scattering rate $1/\tau_\eta(k) = \int S_\eta(k, k') d\vec{k}'$ and introducing the coefficient $\mathscr{A}_\eta = D_\eta^2/(4\pi\rho\omega_\eta)$, we obtain for $\eta = LO, TO$

$$\frac{1}{\tau_\eta(k)} = \frac{2\pi\mathscr{A}_\eta}{(\hbar v_F)^2} \Big\{ N_\eta \left[\varepsilon(\vec{k}) + \hbar\omega_\eta \right] \mathscr{I}^{+,\eta} \\ + (N_\eta + 1) \left[\varepsilon(\vec{k}) - \hbar\omega_\eta \right] \mathscr{I}^{-,\eta} \, \Theta[\varepsilon(\vec{k}) - \hbar\omega_\eta] \Big\}, \quad (5)$$

where $\Theta(x)$ is the Heaviside function, and

$$\mathscr{I}^{\pm,\eta} = \begin{cases} \frac{2\varepsilon(\vec{k}) \pm \hbar\omega_\eta}{\varepsilon(\vec{k}) + (1 \pm 1)\hbar\omega_\eta/2}, & \eta = LO, \\ \frac{\hbar\omega_\eta}{\varepsilon(\vec{k}) + (1 \pm 1)\hbar\omega_\eta/2}, & \eta = TO. \end{cases} \quad (6)$$

We notice that by assuming for $\eta = \{LO, TO\}$ phonons, the same effective scattering parameters[17–20,22,23] $D_\Gamma = D_{op}$ and $\omega_{TO} = \omega_{LO} = \omega_{op}$ and using (5) and (6), we obtain the usual expression $1/\tau_{op} = 1/\tau_{LO} + 1/\tau_{TO}$ used in the MC simulations[17,19,20,23,24] for the optical phonons

$$\frac{1}{\tau_{op}(\vec{k})} = \frac{D_{op}^2}{\rho\omega_{op}(\hbar v_F)^2} \{N_{op} [\varepsilon(\vec{k}) + \hbar\omega_{op}] \\ + (N_{op} + 1) [\varepsilon(\vec{k}) - \hbar\omega_{op}] \Theta[\varepsilon(\vec{k}) - \hbar\omega_{op}]\}. \quad (7)$$

It is easy to verify that, with these assumptions, we can describe equivalently the transverse and longitudinal optical processes as a single optical mode, by using in the sum (2) only a single effective rate[24] $S_{op}(\vec{k}, \vec{k}')$, expressed by (3), with the EPC matrix elements

$$| \mathscr{D}_{op}(\vec{k}, \vec{k}') |^2 = 2D_{op}^2, \quad (8)$$

where factor 2 is due to the presence of both LO and TO branches.

Starting from their DFT results, Borysenko and co-workers[19,20] have found that $K-K'$ intervalley transitions, near the K points, are assisted by TA and LA phonons. However, since in the zone-edge models, there is a significant ambiguity[17,19,20,25] in separating optical or acoustic modes, then, by using a simplified model, also for $K-K'$ inelastic intervalley acoustic transitions, an expression similar to that of optical phonons is considered.[19,20] In particular,

by introducing the same average effective scattering parameters D_{iv} and ω_{iv} for both the interactions with LA and TA modes, the intervalley transfer $1/\tau_{iv} = 1/\tau_{LA} + 1/\tau_{TA}$, takes the same average expression (7) used for the optical phonons[17,19,20]

$$\frac{1}{\tau_{iv}(\vec{k})} = \frac{D_{iv}^2}{\rho\omega_{iv}(\hbar v_F)^2} \{N_{iv} [\varepsilon(\vec{k}) + \hbar\omega_{iv}] \\ + (N_{iv} + 1)[\varepsilon(\vec{k}) - \hbar\omega_{iv}]\Theta[\varepsilon(\vec{k}) - \hbar\omega_{iv}]\}. \quad (9)$$

Therefore, as for intravalley also intervalley transitions are described by a single effective mode and, in sum (2) use is made of a single rate $S_{iv}(\vec{k}, \vec{k}')$, expressed by (3), with the matrix elements

$$| \mathscr{D}_{iv}(\vec{k}, \vec{k}') |^2 = 2D_{iv}^2, \quad (10)$$

where again factor 2 is due to the combined contribution of LA and TA acoustic phonons.

Finally, for the intravalley acoustic scattering, within the elastic-energy-equipartition approximations,[17,19–21] it is $Q_{ac}^{EL} = \int d\vec{k}' \, S_{ac}(\vec{k}, \vec{k}') [\mathscr{F}' - \mathscr{F}]$, where (since there is no distinction between final states obtained by absorption or emission processes), we can write

$$S_{ac}(\vec{k}, \vec{k}') = \mathscr{A}_{ac} (1 + \cos\theta) \delta(\varepsilon' - \varepsilon), \quad (11)$$

where $\mathscr{A}_{ac} = (k_B T_0 D_{ac}^2)/(4\pi\rho\hbar v_s^2)$, with v_s the longitudinal sound velocity, D_{ac} the constant acoustic deformation potential, θ the angle between $\vec{k}$ and $\vec{k}'$, and the term $(1 + \cos\theta)/2$ an analytic squared overlap factor.[17,21] As a consequence, using Eq. (11), we obtain the following expression for the elastic acoustic intravalley scattering rate:

$$\frac{1}{\tau_{ac}} = \int S_{ac}(k, k') \, d\vec{k}' = \frac{D_{ac}^2 k_B T_0}{2\rho\hbar^3 v_s^2 v_F^2} \varepsilon(\vec{k}). \quad (12)$$

We remark that the deformation potential D_{ac} contained in (12) differs by a factor of $\sqrt{2}$ with respect to that proposed in the MC model by Borysenko and co-workers[19,20] (i.e., $D_{ac} = D_{ac}^{(MC)}/\sqrt{2}$). Indeed, in this case, it seems that the authors make use of the "momentum relaxation rate"[17,21,26] instead of the usual "scattering rate" in their MC calculations, multiplying for another factor $1/2$ the expression (12). With these approximations, both the kinetic MC and the macroscopic HD models are quite simplified and, the total rate is expressed as the "effective" average sum $1/\tau_{tot} = 1/\tau_{ac} + 1/\tau_{op} + 1/\tau_{iv}$. Clearly, different choices in the values of the effective parameters ($\{D_{op}, D_{iv}, D_{ac}\}$ and $\{\omega_{op}, \omega_{iv}\}$) imply different values of the numerical results.[17,25] However, we note that the calculations of both the scattering rate and the HD collisional productions require summation over the entire first Brillouin zone (BZ). As a consequence, the scattering parameters used in the MC simulations cannot be calculated only for transitions between particular symmetry points but they must be treated as effective average quantities to determine the contribution of the relevant phonon modes over larger regions of the BZ.[17,19] From these considerations, and to compare the HD results under the same conditions of MC simulations,[20,26–28] in Secs. II B–F, we

consider only two effective inelastic transitions $\eta = \{op, iv\}$ and the elastic acoustic (ac) intravalley processes, with the scattering parameters

$$
\begin{aligned}
&D_{op} = 10^9 \, \text{eV/cm}, \quad \omega_{op} = 164.6 \, \text{meV}, \\
&D_{iv} = 3.5 \cdot 10^8 \, \text{eV/cm}, \quad \omega_{iv} = 124 \, \text{meV}, \\
&D_{ac} = D_{ac}^{(MC)}/\sqrt{2} = (6.8/\sqrt{2}) \, \text{eV}, \\
&\rho = 7.6 \cdot 10^{-7} \, \text{kg/m}^2, \quad v_s = 2.1 \cdot 10^6 \text{cm/s},
\end{aligned}
\tag{13}
$$

as done in MC calculations.[19,20,27,28]

B. Hydrodynamic approach

To pass from the kinetic level of the BTE to the HD level of the balance equations in the framework of the moment theory,[3–6] we consider the following set of kinetic fields $\{1, \varepsilon, u_{i_1}, u_{i_1} u_{i_2}, \dots, u_{i_1} u_{i_2} \dots u_{i_s}\}$, where $s = 1, 2, \dots, M$ with arbitrary values for integer M. Additionally, by using the constraint $\vec{u} \cdot \vec{u} = v_F^2$, as generalized independent kinetic fields, we obtain the unique quantities[29]

$$
\psi_A(\vec{k}) = \{1, \varepsilon, u_{i_1}, u_{\langle i_1 i_2 \rangle}, \dots, u_{\langle i_1 i_2 \dots i_s \rangle}\},
\tag{14}
$$

where $u_{\langle i_1 i_2 \dots i_s \rangle}$ is the traceless part[3–5,11,13,14] of the tensor $u_{i_1} u_{i_2} \dots u_{i_s}$. Given the set (14) of kinetic quantities, for graphene, we obtain a number $\mathcal{N} = 2(M+1)$ of corresponding macroscopic expectation values $F_A = \{F, F_{(1)}, F_{i_1}, F_{\langle i_1 i_2 \rangle}, \dots, F_{\langle i_1 \dots i_s \rangle}\}$, with

$$
F_A = \int \psi_A(\vec{k}) \, \mathcal{F}(\vec{k}, \vec{r}, t) \, d\vec{k},
\tag{15}
$$

where for $M = 1$, we find the usual physical quantities that admit a direct physical interpretation such as $F = n$ (numerical density), $F_{(1)} = W$ (total-energy density), $F_{i_1} = nv_{i_1}$ (velocity flux density). By contrast, for $M > 1$, we obtain macroscopic additional variables of higher order. Multiplying the BTE by the quantities (14) and integrating over k space, in the compact form, we obtain the generalized balance equations for the moments F_A

$$
\frac{\partial n}{\partial t} + \frac{\partial n v_k}{\partial x_k} = 0,
\tag{16}
$$

$$
\frac{\partial W}{\partial t} + \frac{\partial S_k}{\partial x_k} = -e E_k n v_k + P_w,
\tag{17}
$$

$$
\begin{aligned}
&\frac{\partial F_{\langle i_1 i_2 \dots i_s \rangle}}{\partial t} + \frac{\partial F_{\langle i_1 \dots i_s k \rangle}}{\partial x_k} + \frac{v_F^2}{2} \frac{\partial F_{\langle i_1 \dots i_{s-1} \rangle}}{\partial x_{i_s \rangle}} \\
&= e s F_{(-1)|\langle i_1 \dots i_s k \rangle} E_k - \frac{e}{2} v_F^2 s F_{(-1)|\langle \langle i_1 \dots i_{s-1} \rangle} E_{i_s \rangle} \\
&\quad + P_{\langle i_1 i_2 \dots i_s \rangle} \quad \text{with} \quad s = 1, \dots, M.
\end{aligned}
\tag{18}
$$

These equations contain unknown constitutive functions such as (i) the moments of higher order $S_k = \int \varepsilon u_k \mathcal{F} \, d\vec{k}$ (energy flux density) and $F_{\langle i_1 \dots i_M k \rangle} = \int u_{\langle i_1} \dots u_{i_M} u_{k \rangle} \mathcal{F} \, d\vec{k}$; (ii) the external field productions $F_{(-1)|\langle i_1 \dots i_s \rangle} = \int \varepsilon^{-1} u_{\langle i_1} \dots u_{i_s \rangle} \mathcal{F} \, d\vec{k}$, with $s = 0, 1, \dots, M+1$; (iii) the collisional productions, for the total energy density, $P_w = \int \varepsilon Q(\mathcal{F}) \, d\vec{k}$,

and for the remaining tensorial moments, $P_{\langle i_1 \dots i_s \rangle} = \int u_{\langle i_1} \dots u_{i_s \rangle} Q(\mathcal{F}) \, d\vec{k}$, with $s = 1, \dots, M$.

By following the "information theory," all unknown constitutive functions must be obtained, in a self-consistent way, together with the analytic expression for the nonequilibrium distribution function. This problem can be solved by introducing the MEP for a two-dimensional Fermi gas. Once the distribution function is so calculated, all the constitutive functions are determined starting from their kinetic expressions.

C. Applications of MEP and closure relations

In the framework of a local theory, in nonequilibrium conditions, we consider the entropy for an electron gas $S = -k_B \int [\mathcal{F} \ln(\mathcal{F}/y) + y(1 - \mathcal{F}/y) \ln(1 - \mathcal{F}/y)] \, d\vec{k}$. Accordingly, we search the distribution function that maximizes S under the constraints that the expectation values of the moments F_A are expressed by means of Eqs. (14) and (15). The method of Lagrange multipliers[3–6,10–14] proves to be the most efficient technique to include the constraints and solve this variational problem. A short calculation yields the nonequilibrium Fermi distribution[3,4]

$$
\mathcal{F} = \frac{y}{\exp \Pi + 1} \quad \text{with} \quad \Pi = \sum_{A=1}^{\mathcal{N}} \Lambda_A \psi_A,
\tag{19}
$$

where Λ_A is the "Lagrange multipliers" to be determined. The quantities $(19)_2$ can be written explicitly by decomposing them into a "local equilibrium part" $\Pi_E = \alpha + \beta \varepsilon$ and nonequilibrium part $\widehat{\Pi}$, where $\Pi = \Pi_E + \widehat{\Pi}$, with

$$
\widehat{\Pi} = \widehat{\alpha} + \widehat{\beta} \varepsilon + \sum_{r=1}^{M} \widehat{\Lambda}_{\langle i_1 \dots i_r \rangle} u_{\langle i_1} \dots u_{i_r \rangle},
\tag{20}
$$

where α and β are the Lagrange multipliers of local equilibrium, whereas $\{\widehat{\alpha}, \widehat{\beta}, \widehat{\Lambda}_{\langle i_1 \dots i_r \rangle}\}$ denote the nonequilibrium contributions of Λ_A. In particular, by using the "distribution function" $\mathcal{F}|_E = y/[\exp(\alpha + \beta \varepsilon) + 1]$, it is possible to calculate the variables of local equilibrium $n = \int \mathcal{F}|_E \, d\vec{k}$ and $W = \int \varepsilon \mathcal{F}|_E \, d\vec{k}$. Consequently, using these relations, α and β can be obtained as numerical solutions of the system

$$
n = \frac{1}{\gamma \beta^2} I_3(\alpha), \quad \widetilde{W} = \frac{W}{n} = \frac{1}{\beta} \frac{I_5(\alpha)}{I_3(\alpha)},
\tag{21}
$$

with $I_n(\alpha) = \int_0^{+\infty} x^n / [\exp(\alpha + x^2) + 1] \, dx$ being the usual Fermi integral functions[3,4] and $\gamma = (\hbar v_F)^2 / (4\pi y)$. We note that under thermodynamic equilibrium conditions, it is $\beta = (k_B T_0)^{-1}$ and $\mathcal{F}_E$ becomes the usual Fermi distribution at the lattice temperature T_0.

By considering the linear expansion of the distribution function $(19)_1$ around the local equilibrium distribution function $\mathcal{F}_E$, and inserting this expansion in the moment expressions $F_A - F_A|_E = \int \psi_A(\vec{k}) [d\mathcal{F}/d\widehat{\Pi}]_E \widehat{\Pi} \, d\vec{k}$, we can determine analytically the nonequilibrium part of the Lagrange multipliers in the

explicit form

$$\widehat{\alpha} = \widehat{\beta} = 0, \quad \widehat{\Lambda}_{\langle i_1 \ldots i_s \rangle} = -\frac{1}{n} \frac{2^s}{v_F^{2s}} \frac{I_3(\alpha)}{I_1(\alpha)} F_{\langle i_1 \ldots i_s \rangle}, \tag{22}$$

for $s = 1, \ldots, M$. As the MEP distribution function is known, all the constitutive functions can be completely determined in the linear approximation. Thus, we obtain the following:

(i) For the moments of higher order

$$S_k = \frac{2}{\beta} \frac{I_3(\alpha)}{I_1(\alpha)} n v_k, \quad F_{\langle i_1 \ldots i_M k \rangle} = 0. \tag{23}$$

(ii) For the external field productions

$$F_{(-1)} = n\beta \frac{I_1(\alpha)}{I_3(\alpha)}, \quad F_{(-1)|\langle i_1 \ldots i_M k \rangle} = 0, \tag{24}$$

$$F_{(-1)|\langle i_1 \ldots i_s \rangle} = \chi F_{\langle i_1 \ldots i_s \rangle} \quad \text{with} \quad \chi = \frac{\beta/(2I_1)}{e^\alpha + 1} \tag{25}$$

for $s = 1, \ldots, M$.

(iii) For the energy collisional production

$$P_w = n \frac{\pi}{I_3} \left(\frac{\beta}{\hbar v_F} \right)^2 \sum_\eta (\hbar \omega_\eta)^4 \mathscr{A}_\eta \mathscr{H}_\eta \tag{26}$$
$$\times [N_\eta e^{\beta \hbar \omega_\eta} - (N_\eta + 1)],$$

where by introducing the relations

$$L_{0\eta}^\pm(z) = \frac{1}{e^{\pm \alpha \pm \beta \hbar \omega_\eta z} + 1}, \quad L_{1\eta}^\pm(z) = \frac{\partial}{\partial \alpha} L_{0\eta}^\pm(z), \tag{27}$$

the adimensional functions $\mathscr{H}_\eta$ are expressed in the form

$$\mathscr{H}_\eta = 2 \int_0^{+\infty} z(z+1) L_{0\eta}^-(z) L_{0\eta}^+(z+1) \, dz. \tag{28}$$

(iv) Analogously, for the remaining collisional productions, we have, for $s = 1, \ldots, M$,

$$P_{\langle i_1 \ldots i_s \rangle} = - \left[\sum_\eta C^\eta + C_s^{El} \right] F_{\langle i_1 \ldots i_s \rangle}, \tag{29}$$

where the average collision frequencies

$$C^\eta = \frac{\pi}{I_1} \left(\frac{\beta}{\hbar v_F} \right)^2 (\hbar \omega_\eta)^3 \mathscr{A}_\eta \tag{30}$$
$$\times [N_\eta \mathscr{H}^{-,\eta} + (N_\eta + 1) \mathscr{H}^{+,\eta}]$$

account for the inelastic scattering of electrons with different η phonon modes, and using the relations (27), the

adimensional functions $\mathscr{H}^{\mp,\eta}$ are expressed in the form

$$\mathscr{H}^{\mp,\eta} = 2 \int_0^{+\infty} \left\{ L_{0\eta}^+(z + (1 \mp 1)/2) L_{1\eta}^-(z + (1 \pm 1)/2) \right. \tag{31}$$
$$\left. - L_{0\eta}^-(z + (1 \pm 1)/2) L_{1\eta}^+(z + (1 \mp 1)/2) \right\} z(z+1) \, dz.$$

Analogously, the elastic scattering processes with acoustic phonon are described from collision frequencies

$$C_s^{El} = \frac{\mathscr{A}_{ac}}{(\hbar v_F)^2} \frac{4\pi}{\beta} \frac{I_3}{I_1} \mathscr{G}_s \quad \text{with} \quad \mathscr{G}_s = \begin{cases} 1/2, & s = 1, \\ 1, & s > 1. \end{cases} \tag{32}$$

Finally, analyzing the relations (26) and (29), we observe that, as should be expected, at local thermodynamic equilibrium ($F_{\langle i_1 \ldots i_s \rangle} = 0, \ \forall s \geq 1$), all collisional productions vanish, except for P_w, which vanishes only when thermal equilibrium conditions are reached (i.e., $T = T_0$, $\beta = (k_B T_0)^{-1}$ and $[N_\eta \exp(\beta \hbar \omega_\eta) - (N_\eta + 1)]_{T_0} = 0$).

D. Homogeneous conditions

Under homogeneous conditions, due to the axial symmetry, we can take $E_i = \{E, 0\}$ and analogously, for the variables of single-particle $\widetilde{F}_A = F_A/n$, we have $\widetilde{F}_{(1)} = W$, $\widetilde{F}_i = \{v, 0\}$, whereas only the independent components

$$\widetilde{F}_{\langle \underbrace{1 \ldots 1}_{s \text{times}} \rangle} = \widetilde{F}_{\langle s \rangle} \quad \text{for} \quad s = 2, \ldots, M$$

are of concern for the traceless tensorial moment $\widetilde{F}_{\langle i_1 \ldots i_s \rangle}$. Accordingly, the numerical density n assumes a suitable initial constant value, whereas by using Eqs. (16)–(18), we have

$$\dot{\widetilde{W}} = -eEv + \widetilde{P}_w, \tag{33}$$

$$\dot{v} = -eE \left[\frac{v_F^2}{2} \widetilde{F}_{(-1)} - \widetilde{F}_{(-1)|\langle 2 \rangle} \right] + \widetilde{P}_1, \tag{34}$$

$$\dot{\widetilde{F}}_{\langle s \rangle} = -eEs \left[\frac{v_F^2}{4} \widetilde{F}_{(-1)|\langle s-1 \rangle} - \widetilde{F}_{(-1)|\langle s+1 \rangle} \right] + \widetilde{P}_{\langle s \rangle} \tag{35}$$

for $s = 2, \ldots, M$. In this way, the coupled systems (33)–(35) can be expressed in the compact form as

$$\dot{\widetilde{F}}_\alpha = -eE\widetilde{R}_\alpha + \widetilde{P}_\alpha = 0. \tag{36}$$

where $\{\widetilde{F}_\alpha, \widetilde{R}_\alpha, \widetilde{P}_\alpha\}$ are, respectively, the moments, the external field productions, and the collisional productions of the single particle. System (36) is closed, where $\{\widetilde{P}_w, \widetilde{P}_1, \widetilde{P}_{\langle s \rangle}\}$ (for $s = 2, \ldots, M$) and $\{\widetilde{F}_{(-1)}, \widetilde{F}_{(-1)|1}, \widetilde{F}_{(-1)|\langle s+1 \rangle}\}$ (for $s = 1, \ldots, M$) are the single-particle constitutive functions defined in Sec. II C.

E. Conductivity effective mass

In graphene, carriers are considered as massless Fermions. Indeed, from a formal point of view, in none of Eqs. (33)–(35), a mass term appears explicitly. However, as for other physical systems, we can define always a conductivity effective mass $\widetilde{m}$ for the carriers[30,31] as the ratio of the electron momentum $p_i = \hbar k_i$ to its group velocity u_i. In particular, for an isotropic band, $\vec{p}$ and $\vec{u}$ are parallel (n_i being their versor), and, in general, the conductivity effective mass is an increasing function of the microscopic energy $\varepsilon(\vec{k})$.

It is possible to prove that, for any physical system in which $\widetilde{m}$ can be expressed as an increasing function, at least linear in ε, a saturation value c^* for the group velocity $\vec{u}$, is obtained. Accordingly, we can define a "Lorentz factor" $\Gamma = [1 - u^2/(c^*)^2]^{-1/2}$ for the carriers (see Appendix A). In this way, we can rewrite both the microscopic energy and the effective mass in terms of this Γ factor.

In the specific case of monolayer graphene, as a direct consequence of the isotropic linear band structure $\varepsilon(\vec{k}) = \pm \hbar v_F k$, we have $c^* = v_F$, $\Gamma = +\infty$, and

$$\frac{1}{\widetilde{m}} = \frac{v_F^2}{\varepsilon} \quad \text{with} \quad u_i = v_F n_i. \tag{37}$$

With the conductivity effective mass being an increasing function of the energy (i.e., an increasing function of the electric field), and by using Eq. (37)$_1$, we can calculate the "average inverse effective mass" of a single particle

$$\left\langle \frac{1}{\widetilde{m}} \right\rangle = \frac{v_F^2}{n} \int \frac{1}{\varepsilon} \mathscr{F} \, d\vec{k} = v_F^2 \widetilde{F}_{(-1)}, \tag{38}$$

as a decreasing function of the electric field (see the inset in Fig. 3). This quantity is proportional to the constitutive function $\widetilde{F}_{(-1)}$ expressed in local equilibrium conditions and, consequently, Eq. (34) can be rewritten as a function of a usual mass term in the form

$$\dot{v} = -eE\left[\frac{1}{2}\left\langle \frac{1}{\widetilde{m}} \right\rangle - \widetilde{F}_{(-1)|\langle 2 \rangle}\right] + \widetilde{P}_1. \tag{39}$$

We remark that due to the linear band structure, carriers must travel with a velocity of constant modulus [Eq. (37)$_2$]. Therefore, both the electric field and the scattering mechanisms cannot change the modulus of the group velocity, but can only modify its direction n_i. Indeed, if the electric field produces a variation of the electron momentum in the direction of its application, then it tends to align the group velocity (keeping its modulus constant) in the direction of the applied field (see Appendix B). These alignment effects produce an increasing anisotropy of the distribution function, and all moments $\{v_i, \widetilde{F}_{\langle i_1 \dots i_s \rangle}\}$ increase. Analogously, the scattering mechanisms dissipate energy and redistribute momentum in different directions, thus randomizing the group velocity, always keeping its modulus constant. These randomization processes, isotropize the distribution function, and the macroscopic moments $\{v_i, \widetilde{F}_{\langle i_1 \dots i_s \rangle}\}$ decrease. Therefore, an increase or a decrease of these macroscopic quantities is correlated strongly to the combined action of the linear

band structure, of the effective mass, of the external field and of the scattering mechanisms. The delicate equilibrium between these processes can lead, under appropriate conditions, to the onset of a NDM for both the average velocity v_i and the deviatoric moments $\widetilde{F}_{\langle i_1 \dots i_s \rangle}$ also for small or intermediate values of the electric field.

In particular, the role of dissipative phenomena is of fundamental importance to explain the transport phenomena of hot carriers in graphene. Thus, to describe the dynamic, the nature, and the characteristics of dissipative processes, in Sec. II F, we develop a general theory for the small-signal analysis of the hot electrons system.

F. Small-signal analysis

In the framework of the moments approach developed above, the objective of this section is to construct a general theory for a linear-response analysis at a given bias point. Accordingly, under space-homogeneous conditions, we assume that at the initial time, the carrier ensemble is perturbed by an electric field $\delta E \xi(t)$ along the direction of $\mathbf{E}$ [where $\xi(t)$ is an arbitrary function of time satisfying $|\xi(t)| \leq 1$] superimposed to the steady applied field. Then, we calculate the deviations from the stationary values of the moments denoted, respectively, by $\delta\widetilde{F}_\alpha(t)$. Thus, after linearizing Eq. (36) around the stationary state, we obtain the system

$$\frac{d\,\delta\widetilde{F}_\alpha(t)}{d\,t} = \Gamma_{\alpha\beta}\delta\widetilde{F}_\beta(t) - e\delta E\xi(t)\Gamma_\alpha^{(E)}, \tag{40}$$

where all the elements of the "response matrix" $\Gamma_{\alpha\beta}$ and of the "perturbing forces vector" $\Gamma_\alpha^{(E)}$ can be explicitly evaluated starting from the stationary values of the system (see Appendix C). By assuming that $\delta\widetilde{F}_\alpha(0) = 0$, the solution of Eq. (40) is expressed, in terms of the "response vector" $\mathbf{K}(s) = \exp(\Gamma s)\Gamma^{(E)}$, in the form[3,14]

$$\boldsymbol{\delta\widetilde{F}}(t) = -e\delta E \int_0^t \mathbf{K}(s)\xi(t-s)\,ds. \tag{41}$$

The "response functions" $\mathbf{K}(t)$ are real by definition and their initial values can be calculated analytically with $K_\alpha(0) = \Gamma_\alpha^{(E)} = \widetilde{R}_\alpha$ (see Appendix C).

The small-signal analysis is described by the explicit form of the function $\xi(t)$. Thus, we consider two different cases:

(i) Steplike switching perturbation. In this case, $\xi(t) = 1$ for all $t > 0$ and equal to zero otherwise, and we obtain the differential relation

$$K_\alpha(t) = -\frac{1}{e\delta E}\frac{d\delta\widetilde{F}_\alpha}{dt}. \tag{42}$$

It is easy to see that to an extreme position of the perturbation, $\delta\widetilde{F}_\alpha$ corresponds a zero value of K_α and, analogously, that one flex point of $\delta\widetilde{F}_\alpha$ can be associated with an extreme position of the corresponding K_α.

(ii) Harmonic perturbation. In this case, $\xi(t) = \exp(i\omega t)$, and we obtain the harmonic perturbation[3,14] $\boldsymbol{\delta\widetilde{F}}(t) = \boldsymbol{\delta\widetilde{F}}(\omega)\exp(i\omega t)$

with $\delta\widetilde{F}_\alpha(\omega) = \mu'_\alpha(\omega)\delta E$, where

$$\mu'_\alpha(\omega) = -e \int_0^\infty K_\alpha(s) \exp(-i\omega s) \, ds \qquad (43)$$

is the moment generalized ac differential mobility, a complex quantity, with the imaginary part being associated with the reactive contribution. The explicit forms of $\Gamma_\alpha^{(E)}$ and $\Gamma_{\alpha\beta}$, for the monolayer graphene, are reported in Appendix C. Besides, by using some analytical expressions given in the Appendix [Eqs. (C5)–(C13)], an anatomy of both the response functions and differential mobilities can be inferred, including their connections with the streaming character of carriers, with the dissipative processes and with the dc NDM of moments.

III. HD NUMERICAL RESULTS

In this, section theory is applied to the case of electrons in monolayer graphene at $T = 300\,\mathrm{K}$ in a wide range of electric fields up to $80\,\mathrm{kV/cm}$ and carrier concentration 5×10^{11}–$1 \times 10^{13}\,\mathrm{cm}^{-2}$.

A. Collision frequencies

Following the present approach, and using the relations (21), all collision frequencies (30) and (32) can be expressed as functions of the local equilibrium variables $\{n, \widetilde{W}\}$. Besides, by considering the effective inelastic transitions $\eta = \{op, iv\}$, with the model proposed by Borysenko and co-workers,[19,20] we obtain a unique collision frequency C^η both for the velocity v and for all remaining deviatoric moments $F_{\langle s \rangle}$.

Figure 1 reports the mean collision frequencies C^{op}, C^{iv}, C_1^{El} (see the inset in Fig. 1) as function of electron average-energy $\widetilde{W}$ for different electron densities. From an analysis of the mean collision frequencies, we find that (i) the contribution of emission processes is dominant with respect to the contribution of absorption processes in the range of considered electric-field; (ii) by using the deformation
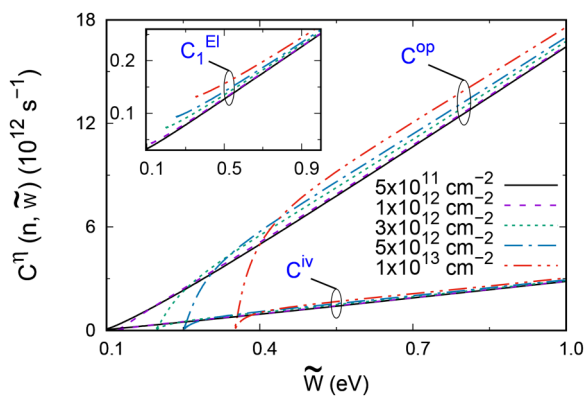

FIG. 1. Collision frequencies $\{C^\eta, C_1^{El}\}$ [Eqs. (30) and (32)] vs average energy $\widetilde{W}$ for increasing electron density n. By using (13) for the inelastic transitions $\eta = \{op, iv\}$, we obtain an unique collision frequency $C^\eta = C_s^\eta$ ($s = 1 \ldots M$) both for the velocity v and for all remaining deviatoric moments $\widetilde{F}_{\langle s \rangle}$.

potentials (13), the elastic intravalley collisions are negligible with respect to the inelastic collisions, where $C^\eta \gg C_s^{El}$ for $\eta = \{op, iv\}$ and $s \geq 1$ [see the inset in Fig. 1 and Eq. (32)]. Analogously, by considering the collision frequencies for the inelastic transitions, the optical (op) intravalley transitions prevail with respect to the intervalley (iv) transitions, although these latter remain not negligible.

(iii) For low electron densities ($n = 5 \times 10^{11}\,\mathrm{cm}^{-2}$ and $n = 10^{12}\,\mathrm{cm}^{-2}$) and in correspondence with low energies (i.e., for low electric fields), all collision frequencies increase slowly keeping very small values. Thus, we have a few number of collisional processes and, consequently, the effects imputable to the electric field prevail with respect to those of scattering processes. By contrast, for high electron densities ($n = 3 \times 10^{12}\,\mathrm{cm}^{-2}$; $n = 5 \times 10^{12}\,\mathrm{cm}^{-2}$; $n = 10^{13}\,\mathrm{cm}^{-2}$), the collision frequencies increase very fast starting from low energies, near to the equilibrium conditions[32] (Fig. 1). Consequently, for high electron densities the initial effects, due to the electric field, are strongly reduced by dissipation processes, already starting from very small values of E. These results suggest that, as for the collisional frequencies, also the behavior of corresponding macroscopic moments will be strongly dependent on the electron density, for small E values.

(iv) For increasing values of the electric field, the driving field couples with the scattering processes and we assist, due to the linear band structure, to a further increase of the scattering efficiency. In particular, for high electric fields, the behavior of the collisional frequencies is essentially the same for all the electron densities. Indeed, for both high and low electron densities, at increasing energy all collision frequencies increase very fast, in an approximately linear way, with the energy (or, equivalently, in an approximately linear way with E; see the energy in Fig. 4). In this case, we expect that also the behavior of the corresponding macroscopic moments is almost independent on electron density, with moments-field curves that are converging toward each other for very high fields values.

B. HD stationary calculations

By fixing the values of n and M, for any single simulation, HD systems (33)–(35) are solved numerically, under stationary conditions, for about 100 values of electric field E in the range $\mathscr{H} = [0, 80]\,\mathrm{kV/cm}$.

All simulations are performed by using an increasing number of moments (i.e., by increasing progressively the value of M) until a final convergence of numerical results within 1% is achieved. In this respect, it should be noted that for any single simulation, also using a large number of moments (for example, $M \approx 50, 60$), all HD results are obtained with computational times shorter than 1 min on a standard workstation.

In general, we have verified the following:

(i)   The energy-field curves converge much more quickly than the velocity-field curves.
(ii) For increasing values of M, all numerical HD results converge to the same final values and are in good agreement with the corresponding MC results.
(iii) The number of moments necessary to obtain the final convergence (in particular, for the velocity-field curves) is inversely proportional to the electron density considered.

Thus, to estimate the final convergence of the velocity-field curves $v_M(E)$, we have solved HD systems (33)–(35) for different values of M and $E \in \mathscr{H}$. Consequently, for any parametrized electron density, we have evaluated the "maximum relative error"

$$\Delta_M^{(v)} = \max_{E \in \mathscr{H}} \left| \frac{v_M(E) - v_{M+1}(E)}{v_{M+1}(E)} \right| \quad (44)$$

in correspondence with increasing values of M.

Figure 2 shows, in a systematic way, the "maximum percentage error" $\Delta_M^{(v)} \times 100$ for the calculation of the average velocity v as function of the number of moments used at different electron densities. The final numerical convergence of the average velocity shows evident variations, for increasing values of the integer number M, only at low electron densities. Thus, to obtain an excellent convergence (i.e., a "maximum percentage error" below 1%), we must consider $M \approx 50$ for $n = 5 \times 10^{11}\,\mathrm{cm^{-2}}$ and $M \approx 22$ for $n = 10^{12}\,\mathrm{cm^{-2}}$. By contrast, at higher electron densities, a very small number of moments ($M \approx 8$ for $n = 3 \times 10^{12}\,\mathrm{cm^{-2}}$, $M \approx 6$ for $n = 5 \times 10^{12}\,\mathrm{cm^{-2}}$, and $M = 4$ for $n = 10^{13}\,\mathrm{cm^{-2}}$) are needed to obtain an excellent convergence of HD results. We remark that the final convergence of the velocity is closely related with the external field production R_v entering Eq. (39). Thus, in Fig. 3, we report $\widetilde{R}_v$ and, separately, its constituent parts $\langle 1/\widetilde{m} \rangle$ (see the inset) and $\widetilde{F}_{(-1)|\langle 2 \rangle} = \chi \widetilde{F}_{\langle 2 \rangle}$ as function of the electric field at different electron densities. For low electron densities ($n = 5 \cdot 10^{11}\,\mathrm{cm^{-2}}$), the terms $(1/2)\langle 1/\widetilde{m} \rangle$ and $\widetilde{F}_{(-1)|\langle 2 \rangle}$ are of comparable value. Thus, Eqs. (33) and (39) for $\widetilde{W}$ and v are strongly coupled with the HD equations (35) for the remaining deviatoric moments $\widetilde{F}_{\langle s \rangle}$. In this case, the use of many moments is necessary to obtain an excellent final convergence of the velocity v. By contrast, for high electron densities ($n = 10^{13}\,\mathrm{cm^{-2}}$), it is possible to verify that, the mass term $\langle 1/\widetilde{m} \rangle$ is predominant (i.e., $\langle 1/\widetilde{m} \rangle \gg \widetilde{F}_{(-1)|\langle 2 \rangle}$). In this case, the equations for $\widetilde{W}$ and v are weakly coupled[33] with the remaining HD equations (35) and, consequently, only few moments suffice to obtain an excellent final convergence of the average velocity.

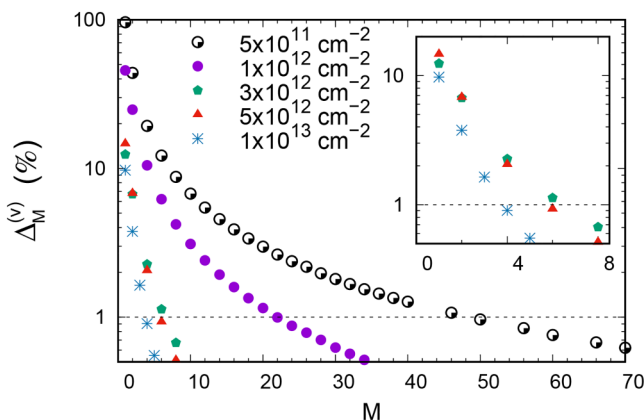**FIG. 2.** Maximum percentage error $\Delta_M^{(v)} \times 100$ for the calculation of velocity v, as function of the integer M [see Eq. (44)], for different parametrized electron densities.
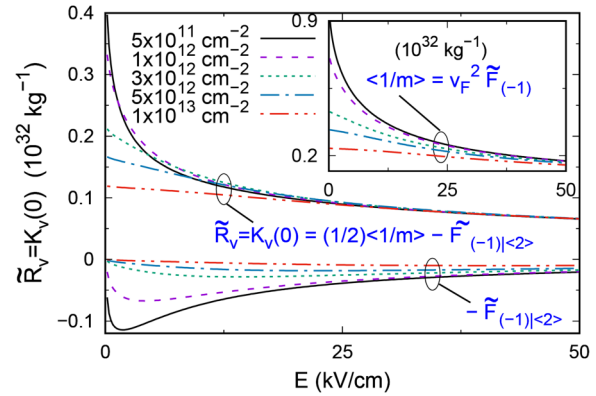
FIG. 3. External field production $\widetilde{R}_v = \Gamma_v^E = K_v(0)$ contained in the HD Eq. (39) [see also Eq. (C2)] for the velocity v, as function of electric field E for different electron densities.

Figure 4 reports the HD and the MC results for the average velocity v and energy $\widetilde{W}$ as a function of the electric field for two values of electron density $n = 5 \cdot 10^{11}\,\mathrm{cm^{-2}}$ and $n = 10^{12}\,\mathrm{cm^{-2}}$. Lines refer to present HD results obtained under stationary conditions, for different values of M. Symbols (stars and circles) refer to MC calculations available from the literature[20,27,28] and obtained in the same physical conditions of HD calculations (i.e., by using the same scattering terms with the same scattering parameters). The HD results exhibit a significant dependence on the number of moments used and this is particularly evident for the velocity.[34] In general, for the first odd values of M (see, for example, the case $M = 1$ with the moments $\{W, v\}$) HD results are overestimated with respect to those of MC. By contrast, for the first even values of M (see, for example, the case $M = 2$ with the moments $\{W, v, F_{\langle 2 \rangle}\}$) HD numerical results are underestimated when compared to those of MC. In any case, for increasing values (even or odd) of M, HD calculations converge to the same final values and the achieved good agreement with MC data validates the present HD-MEP approach.

Figure 5 shows, in a systematic way, the final convergence of the HD numerical calculations, under stationary conditions, for both the average velocity v and average energy $\widetilde{W}$ as a function of the electric field in a wide range of values ($E \in [0, 80]\,\mathrm{kV/cm}$), parametrized by different electron densities. In general, we have verified the following:

(i)   The average velocity exhibits a different saturation trend in correspondence with an increasing electron concentration, with the onset of a NDM more pronounced at low carrier densities.

Accordingly, at lower electron density, the value of the peak velocity is higher, the onset of NDM occurs at lower electric fields, and the NDM is maintained also at low fields. This behavior is well confirmed by most theoretical studies existing in the literature.[17,20,23] In particular, we observe the onset of NDM for fields of approximately $2-3\,\mathrm{kV/cm}$ at low densities ($n = 5 \cdot 10^{11}\,\mathrm{cm^{-2}}$, $n = 10^{12}\,\mathrm{cm^{-2}}$), but this NDM almost disappears at densities higher than about $10^{13}\,\mathrm{cm^{-2}}$.

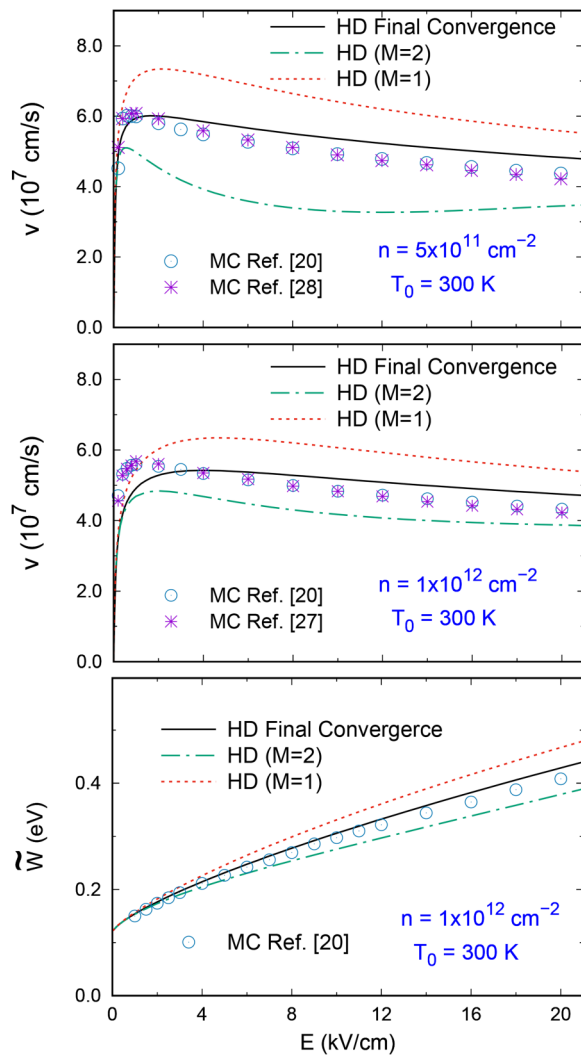**FIG. 4.** Drift velocity v vs electric field E for electron densities $n = 5 \times 10^{11}$ cm^{-2} and $n = 10^{12}$ cm^{-2}. Average energy $\widetilde{W}$ for $n = 10^{12}$ cm^{-2}. Lines refer to HD results obtained by solving Eqs. (33)–(35) with different values of M. Symbols (open circles and stars) refer to MC simulations (Refs. 20, 27, and 28).
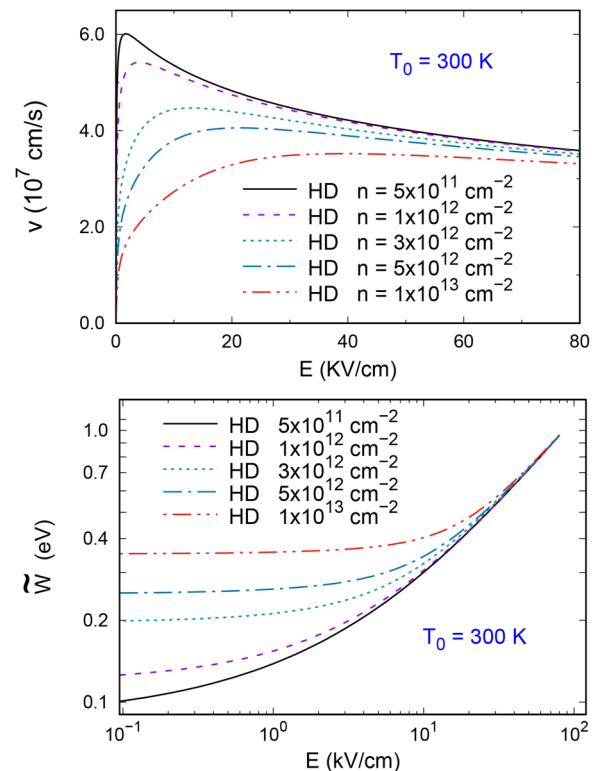

FIG. 5. Final convergence of the HD numerical results, obtained for different electron densities. In particular, we report, in linear scale, the velocity v and analogously, in logarithmic scale, the energy $\widetilde{W}$ in function of the electric field E.

(ii) Regarding the average energy parametrized by different carrier densities, the energy-field curves start from their thermal equilibrium value at the lowest fields and then converge to the same linear asymptotic trend at the highest fields, a behavior correlated with the peculiar energy dispersion of the band (see Fig. 5).

(iii) As shown in Fig. 6, the deviatoric moments $F_{\langle s \rangle}$ show a behavior analogous to that of the average velocity v. Indeed, for low electron densities and for increasing values of s, the moments $F_{\langle s \rangle}$ exhibit a strong initial increase, then tend to saturate, by decreasing at the highest electric fields with a "generalized differential mobility" that takes negative values.

In particular, also in this case, we observe the onset of a NDM for small values of the electric field and at low carrier densities, while the NDM of these moments almost disappears at densities higher than about 10^{13} cm^{-2}.

To provide a physical interpretation of the curves reported in Figs. 1–6, it is useful to analyze the different contributions that can be associated with the separate actions of the scattering mechanisms, of the electric field and of the band structure. In particular,

(i) For low electron densities ($n = 5 \cdot 10^{11}$ cm^{-2} and $n = 10^{12}$ cm^{-2}), near to thermal equilibrium conditions, all collision frequencies increase slowly and are very small. Therefore, for low electric fields, we have a few number of collisional events that, as we will see, will lead to the onset of a streaming motion regime. In this case, the effects imputable to the electric field will prevail over the effects due to scattering phenomena. Consequently, the energy increases, the electric field tends to align the group velocity in the direction of the applied field (see Appendix B), by keeping its modulus constant, but producing an increasing anisotropy in the distribution function.[15] In correspondence with this anisotropy, both the average velocity v and the macroscopic deviatoric moments $\widetilde{F}_{\langle s \rangle}$ increase rapidly for very small electric fields. When the electric
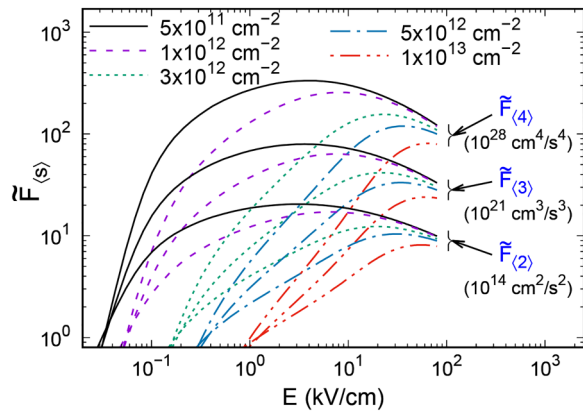
FIG. 6. Final convergence of the HD numerical results, for the deviatoric moments $\{\widetilde{F}_{\langle 2 \rangle}, \widetilde{F}_{\langle 3 \rangle}, \widetilde{F}_{\langle 4 \rangle}\}$ obtained, for different electron densities n, as functions of field E, at $T_0 = 300\,\mathrm{K}$.

field increases further, we assist to an increase of the scattering rate. In this case, the applied field acts mainly on the energy, while the scattering mechanisms act mainly on the velocity and on the deviatoric moments. Thus, for increasing values of the electric field, the energy $\widetilde{W}$ increases faster because of the reduced efficiency of scattering to dissipate the excess energy gained by the field. By contrast, v and $\widetilde{F}_{\langle s \rangle}$ show saturation phenomena, with a subsequent marked an NDM, because of the enhanced efficiency of scattering to dissipate through randomization the momentum gained by the field. In this case, starting from the onset of the NDM, the effects imputable to scattering phenomena will prevail over he effects due to electric field. Indeed, the collisional processes will produce an increasing randomization of the group velocity which, keeping its modulus constant, tends to isotropize the distribution function. Consequently, the macroscopic variables $\{v, \widetilde{F}_{\langle s \rangle}\}$ will decrease at increasing values of the electric fields.

(ii) For higher values of electron density ($n = 3 \cdot 10^{12}\,\mathrm{cm}^{-2}$, $n = 5 \cdot 10^{12}\,\mathrm{cm}^{-2}$, and $n = 10^{13}\,\mathrm{cm}^{-2}$), the collision frequencies are rapidly increasing near to thermal equilibrium conditions. In this way, there is a comparatively larger number of scattering events at low electric field values, and all moments are strongly affected by dissipative phenomena also for very small electric fields. Therefore, for high electron densities and small electric fields, the average energy W grows very slowly near thermal equilibrium conditions (Fig. 5), while for increasing values of the electric fields, the effects of the applied field prevail on scattering mechanisms and (as in the case of low electron densities) the energy-field curves increase rapidly, converging toward each other at high fields.

Analogously, for both the average velocity and the deviatoric moments, the initial effects due to the electric field (which tend to align the group velocity in the direction of applied field) are strongly attenuated by the scattering mechanisms which, vice versa, by randomizing the group velocity, tend to isotropize the distribution function. Thus, v and $F_{\langle s \rangle}$ increase slower and

are lower in correspondence of a higher electron density. Subsequently, through the increasing dissipation phenomena, we observe the saturation effects with an onset of the saturation moved forward and, consequently, a NDM strongly attenuated with increasing electron density (to the point of practically disappearing at densities higher than about $n = 10^{13}\,\mathrm{cm}^{-2}$).

(iii) For very high energies, both the behavior of the electric field and the behavior of scattering mechanisms are essentially independent on the electron density. As a direct consequence, also behavior of corresponding macroscopic moments is almost independent of electron density, with moments-field curves that are converging toward each other for very high fields values.

C. HD small-signal analysis

In order to describe the nature of dissipative phenomena for the electron system, we consider the study of the eigenvalues of the response matrix, the analysis of the time decay of the "response functions" and the spectrum of the corresponding "ac differential mobilities."

In general, the eigenvalues of the response matrix $\Gamma_{\alpha\beta}$ are complex quantities with the imaginary part indicating the presence of some kind of "deterministic" relaxation in the system that can be attributed to a "streaming character" of the distribution function. Figure 7 reports the generalized relaxation rates $v_\alpha = -\lambda_\alpha$ both for the velocity v and the energy $\widetilde{W}$ as a function of electric field, obtained with $M = 1$, for different electron densities. The velocity and energy relaxation rates are coupled reciprocally for almost the entire extension of values of the considered electric field. The complex eigenvalues have the same real part with an imaginary part comparable with the real part in a large part of coupling region. Only for very small electric fields, $-\lambda_v$ and $-\lambda_w$ are decoupled, and in this case, the coupled region is more extensive if the electron density is smaller (see the inset in Fig. 7). For increasing values of M, the $\Gamma_{\alpha\beta}$ spectrum behavior becomes sufficiently intricate because we can observe also some coupling regions associated with deviatoric moments $\widetilde{F}_{\langle s \rangle}$.
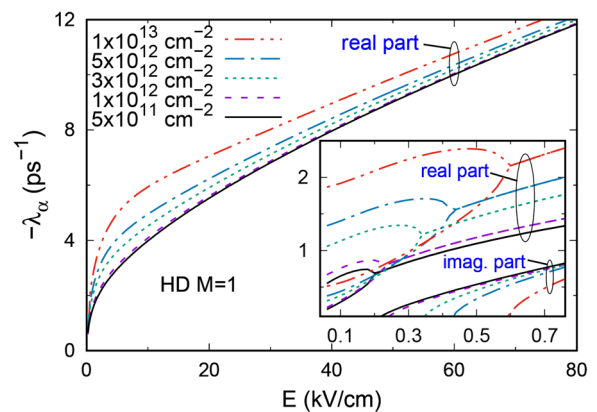

FIG. 7. Eigenvalues of the relaxation matrix $\Gamma_{\alpha\beta}$ vs electric field. The lines refer to the real parts of the eigenvalues associated, respectively, to the velocity v and energy $\widetilde{W}$, evaluated for different electron densities with $M = 1$. In the inset we report, only for very low fields, also the imaginary parts.

However, we have verified that, by considering a increment of M, the essential characteristics of the spectrum shown in Fig. 7 remain unchanged. Therefore, the analysis of the generalized relaxation rates $-\lambda_\alpha$ shows that the electron transport in graphene is essentially characterized by a streaming motion regime imputable to the combined action of the electric field and of the scattering phenomena. This behavior is evident for any electron density, with an onset of the streaming motion regime obtained by starting from very low electric fields values $(0.2-0.6\,\text{kV/cm})$. The streaming motion is particularly evident also in the presence of a few number of collisional events (i.e., low electron densities and very small electric fields) and it extends to larger values than in the case of usual semiconductors.[3,14,15]

In Figs. 8 and 9, we report the response functions $K_v(t)$ and $K_{\widetilde{W}}(t)$, and in the insets, the corresponding differential responses $\delta v/\delta E$ and $\delta \widetilde{W}/\delta E$ to a steplike switch-on of the electric field, for two different electron densities $(n = 5 \cdot 10^{11}\,\text{cm}^{-2}$ and $n = 10^{13}\,\text{cm}^{-2})$, at increasing electric fields. Each curve $K_v(t)$, in Fig. 8, is normalized to its initial value to allow for a comparison of the different decay-time scales. By using Eqs. (C2), the initial values $K_v(0) = \Gamma_v^{(E)} = \widetilde{R}_v$ are explicitly reported in Fig. 3 as positive decreasing functions of electric field. In particular, for low electron densities and for low electric fields, the $K_v(0)$ curves decrease
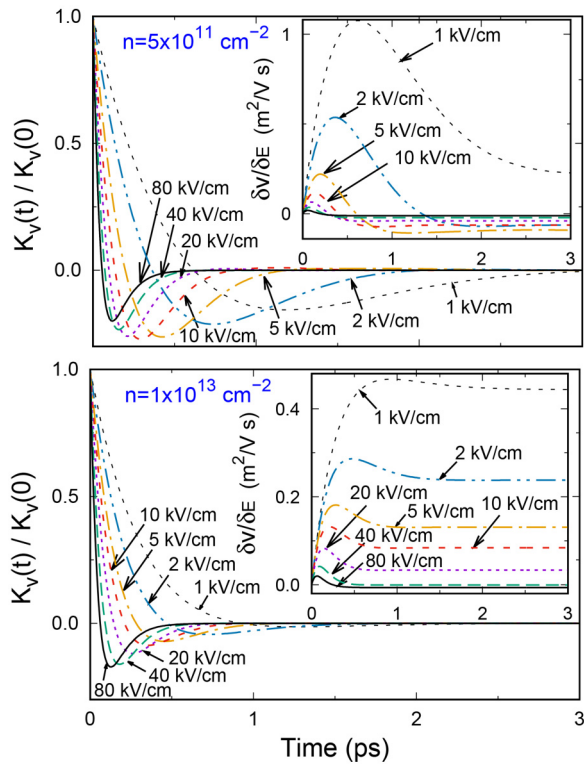

FIG. 9. Time dependencies of the response functions $K_{\widetilde{W}}$ and, in the inset, of the corresponding differential response $\delta \widetilde{W}/\delta E$ to a steplike switch-on of the electric field, obtained for graphene with two different electron densities $(n = 5 \cdot 10^{11}\,\text{cm}^{-2}, n = 10^{13}\,\text{cm}^{-2})$ and for increasing electric fields.
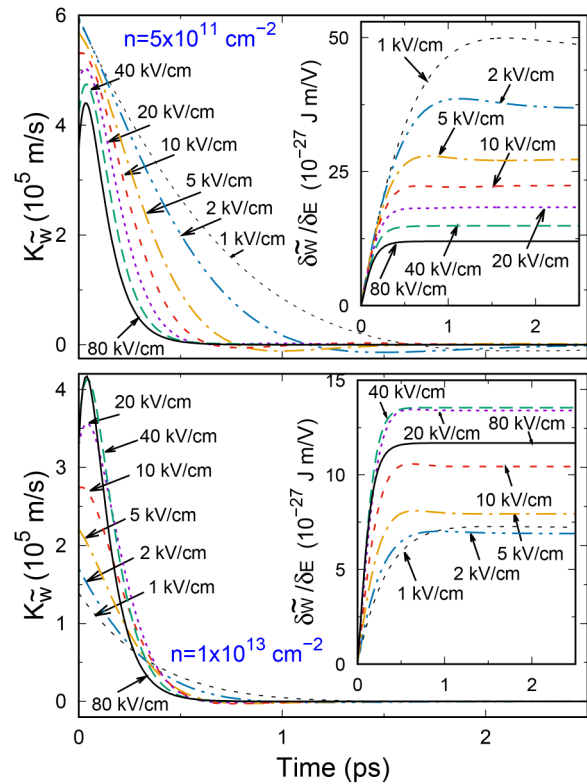
rapidly while, by contrast, for all electron densities considered and for high fields, the curves converge toward each other assuming values slowly decreasing (behavior imputable, essentially, to the mass term $\langle 1/m \rangle$). The curves $K_{\widetilde{W}}(t)$ reported in Fig. 9 are not normalized and, from Eq. (C1), the initial values $K_{\widetilde{W}}(0) = v$ are very different, for the two electron densities, because the behavior of velocity v is different in correspondence of the same values of the dc electric fields (see Fig. 5). In general, from Figs. 8 and 9, we observe that for small electric fields $(E = 1 - 2\,\text{kV/cm})$, the response functions, associated with electron density $n = 5 \cdot 10^{11}\,\text{cm}^{-2}$, decay much slower with respect to the curves obtained in correspondence of a much higher electron density $n = 10^{13}\,\text{cm}^{-2}$. These results confirm that, for low electric fields and for low electron densities, we have a small number of collisional processes, and, consequently, in the electron transport, the alignment effects of group velocity, due to electric field, will prevail with respect to randomization processes imputable to scattering mechanisms.

Figure 8 shows, in a systematic way, that the combined action of the electric field and dissipative processes induces a nonexponential decays of the $K_v(t)$ curves by exhibiting a negative part that implies an overshoot of the corresponding differential response. Thus, the

FIG. 8. Time dependencies of the normalized response functions K_v and, in the inset, of the corresponding differential response $\delta v/\delta E$ to a steplike switch-on of the electric field, obtained for graphene with two different electron densities $(n = 5 \times 10^{11}\,\text{cm}^{-2}, n = 10^{13}\,\text{cm}^{-2})$ and for increasing electric fields.

perturbations $\delta v / \delta E$ quickly increase with time when $K_v(t) > 0$, reach a maximum at time $\bar{t}$ corresponding to $K_v(\bar{t}) = 0$, and then decay asymptotically toward the steady state when $K_v(t) < 0$. We remark that, if the negative part of response function $K_v(t)$ is relevant, then this behavior is certainly connected with the onset of the dc NDM for the velocity, and, consequently, with the prevalence of the dissipations effects with respect to effects due to the electric field. Indeed, by considering regions with a NDM (see Fig. 5) for the velocity v ($E \geq 2\,\text{kV/cm}$ for $n = 5 \cdot 10^{11}\,\text{cm}^{-2}$) from Eq. (C7), we obtain $X_v(0) \leq 0$ (zero at the onset of NDM), and analogously, the integral in Eq. (C9) must be negative or null. Thus, if the initial part of the response functions $K_v(0)$ is positive (see Fig. 3), then at long times the contribution of the integrand in Eq. (C9) must be negative to compensate. In this transition, the response functions fall down through a zero and the corresponding derivative becomes negative. In particular, if at the transition point it is $dK_v / dt < 0$, then, from Eq. (42) to a zero value of K_v, it corresponds a positive maximum of δv (see the inset in Fig. 8), and analogously [using the derivative of Eq. (42)], to one flex point of the perturbation δv (see the inset) can be associated a minimum of the corresponding response function. In particular, in the presence of a NDM for v, the corresponding perturbations $\delta v / \delta E$, after passing the flex points, must decay necessarily toward a "negative" steady state (see the inset in Fig. 8). Therefore, the negative part of the response function $K_v(t)$ is associated with the combined action of the electric field and dissipative processes, and it predominates in the integral (C9) when the effects of collisional processes predominate on the effects of the electric field [i.e., in the presence of a NDM, when $X_v(0) \leq 0$]. However, for continuity reasons, the previous behavior of the functions $K_v(E, t)$ must be valid also in some range of lower electric fields. Thus, for $E = 1\,\text{kV/cm}$ and $n = 5 \cdot 10^{11}\,\text{cm}^{-2}$, the response function K_v still shows a large negative part, highlighting the "streaming motion regime" in the electron transport, also in the presence of a few number of collisional events. Of course, in this case, $X_v(E, 0) > 0$, the positive values of the integrand in (C9) will be predominate, and the electric field effects will prevail on the collisions effects. We remark that, also the energy response function $K_{\widetilde{W}}$ evidences the streaming character of hot carriers. In particular, as in the usual semiconductors,[3,14,35] for intermediates and high values of electric field ($E \geq 10\,\text{kV/cm}$ in Fig. 9), the $K_{\widetilde{W}}$ curves show a non-monotonic behavior with a maximum (for $\tilde{t} \neq 0$), which separates different time scales, indicating the onset of a diffusive regime for $t > \tilde{t}$. For low electric fields, the maximum value of $K_{\widetilde{W}}$ moves to the left at $\tilde{t} = 0$ by showing that, in this case, we have only the onset of an immediate streaming motion regime for $t > 0$.

Figures 10 and 11 report the spectra of the ac differential mobility μ'_v, associated with the velocity v, for the two different electron densities $n = 5 \cdot 10^{11}\,\text{cm}^{-2}$ and $n = 10^{13}\,\text{cm}^{-2}$. Also the $\mu'_v(\omega)$ curves show similar common features, by reflecting the behavior of the corresponding response functions. Indeed, in the presence of dissipative processes, the distinctive behavior of all functions K_v evidence an initial drop with an "overshoot to negative values." If the overshoot is enough pronounced, then the negative values of the integrand functions $tK_v(t)$ and $t^2 K_v(t)$ must predominate in the integrals (C10) and (C11). Thus, from Eq. (C8)$_1$, the real part of curves μ'_v must increase[36] through a maximum before decreasing toward its high-frequency limit of Eq. (C12)$_1$. The height of the
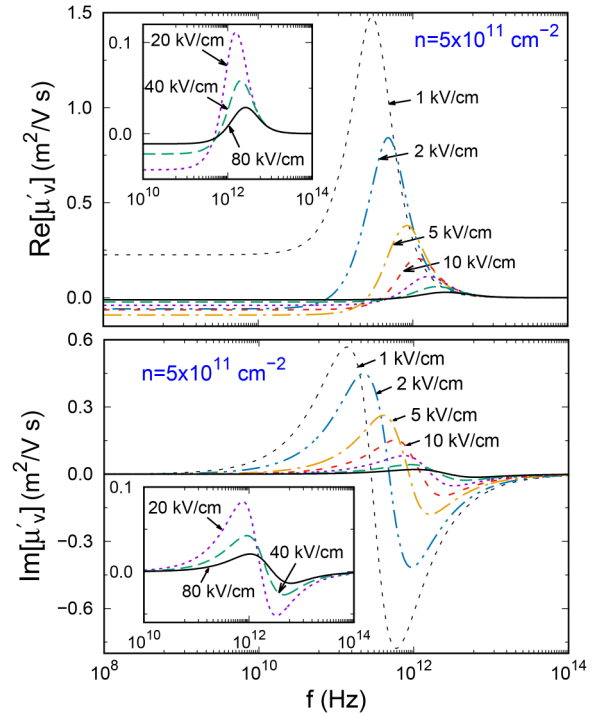

FIG. 10. Real and imaginary parts of the ac differential mobility μ'_v for the velocity v as functions of the frequency f at a low electron density $n = 5 \cdot 10^{11}\,\text{cm}^{-2}$ at $T_0 = 300\,\text{K}$ and increasing dc electric fields.

peaks increases for low electron densities, because it is connected with the amplitude of the negative parts of response functions, while the position of the peaks slightly shifts to higher frequencies at increasing fields. Analogously, from Eq. (C8)$_2$, also the shape of curves $\text{Im}[\mu'_v]$ must be initially positive while, being $K_v(0) > 0$ from Eq. (C12)$_2$, the imaginary parts must be negative in some frequency range extending to infinity. Therefore, if the negative part of curves K_v is relevant, we find that at low frequencies $Y_\alpha(\omega) > 0$, at intermediate frequencies $Y_\alpha(\omega) = 0$, and for some range of frequencies extending to infinity $Y_\alpha(\omega) < 0$.

We have thus established that the negative parts of response functions K_v, the positive overshoots of the corresponding differential responses $\delta v / \delta E$, the peaks of real parts $\text{Re}[\mu'_v]$, and the maxima (with the consequent fall through a zero) of the imaginary parts $\text{Im}[\mu'_v]$ all describe the same dissipative microscopic phenomena. These correlations are particularly evident when the negative part of K_v is relevant, and we observe in correspondence a dc NDM for the velocity v (i.e., when $X_v(0) < 0$).

By considering the remaining deviatoric moments $\widetilde{F}_{\langle s \rangle}$, we have verified that at increasing values of s, all functions $\{K_{\langle s \rangle}, \delta \widetilde{F}_{\langle s \rangle} / \delta E, \mu'_{\langle s \rangle}\}$ exhibit a very similar evolution to that of the functions $\{K_v, \delta v / \delta E, \mu'_v\}$ for the velocity. In particular, also in this case, in correspondence of a generalized NDM (see Fig. 6), the negative parts of the response functions $K_{\langle s \rangle}$ are predominant in the
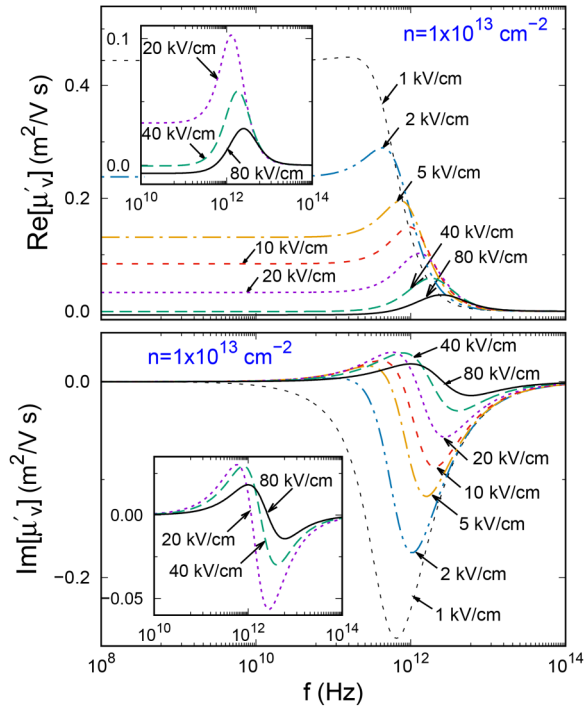
FIG. 11. Real and imaginary parts of the ac differential mobility μ'_v for the velocity v as functions of the frequency f for a very high electron density $n = 10^{13}$ cm^{-2} at $T_0 = 300$ K and increasing dc electric fields.

time domain, at increasing frequencies all curves Re[$\mu'_{\langle s \rangle}$] exhibit a peak before falling off to zero and, analogously, all the imaginary parts Im[$\mu'_{\langle s \rangle}$] increase through a positive maximum before decreasing toward a negative minimum.

Lastly, for high fields ($E = 80$ kV/cm), the response functions $\{K_v, K_{\widetilde{W}}, K_{\langle s \rangle}\}$ the differential responses $\{\delta v, \delta \widetilde{W}, \delta \widetilde{F}_{\langle s \rangle}\}$, and the corresponding ac differential mobilities $\{\mu'_v, \mu'_{\widetilde{W}}, \mu'_{\langle s \rangle}\}$ are substantially the same for the two different electron densities (see Figs. 8–11). In this case, the behavior of scattering mechanisms is essentially independent of the electron density and, as direct consequence, also the dynamic, the nature, and the characteristics of dissipative processes, expressed in the framework of small-signal analysis, are the same in the case of very high electric fields.

IV. CONCLUSIONS

By using the MEP, we have presented a general theory to analyze high-field transport in monolayer graphene. The theory is formulated, at a kinetic level, without the need to introduce external parameters. To this purpose, the simplified model proposed by Borysenko and co-workers[19,20] has been used for the scattering mechanisms, with scattering parameters that appear to have been averaged over large regions of the BZ.[17,19] Therefore, by using the MEP in a dynamic contest, we have constructed a closed HD system containing all underlying physical processes in an explicit

way. In homogeneous and stationary conditions, the HD results show that the behavior of all moments is imputable to the linear band structure and to the competition between the effects induced by the external field and the effects induced by scattering mechanisms. This competition depends, essentially, on the parametrized electron density, and, in general, while the action of an increasing electric field prevails on the energy $\widetilde{W}$ by contrast, the effects of dissipative processes are more evident on the velocity v and in the deviatoric moments $\widetilde{F}_{\langle s \rangle}$.

In the specific case of monolayer graphene, due to the linear band, both the average velocity and all deviatoric moments are expressed as an ensemble average of the versors n_i associated with the group velocity. Besides, we have shown that the peculiar condition $u_i = v_F n_i$, together with an effective mass increasing with the energy, induces the electric field to align the carriers microscopic velocities (keeping their modulus unchanged) in the direction of the applied field. Vice versa, all scattering mechanisms (elastic and anelastic) randomize the group velocity (always keeping its modulus unchanged) and, consequently, an increasing collisional frequency (i.e., an increasing number of collisional events) produces, on the group velocity, a directional effect opposite to that induced by the electric field. When the alignment effects prevail on the randomization processes, then, we have an increasing anisotropy of the distribution function in the direction of applied field and the moments $\{v, \widetilde{F}_{\langle s \rangle}\}$ increase. Vice versa, if the scattering mechanisms prevail with respect to the electric field alignment effects, then the randomization processes tend to isotropize the distribution function, and the moments decrease. The processes described above occur, more or less incisively, for any values of electric field, but are particularly evident in correspondence of low electron densities and of low electric fields, when the alternation and the competition between these processes can lead to the onset of a NDM both for the average velocity v and for the deviatoric moments $\widetilde{F}_{\langle s \rangle}$. Since, for very low electric fields, the number of collisional events is strongly dependent on the electron density, then, as a direct consequence, the behavior of the NDM will strongly depend on the carrier density. Vice versa, for high electric fields, the behavior of scattering mechanisms is essentially independent of the electron density, and, consequently, the behavior of the corresponding macroscopic moments is almost independent of electron density, with the moments-field curves that tend to converge, mutually, toward each other. Besides, by investigating the nature of dissipative processes, we have shown that the electron transport is characterized by the streaming motion regime due to the combined action of the electric field and scattering phenomena. The streaming motion is also present in the presence of a few collisional events (i.e., low electron density and very small electric fields) and it extends to larger values of the external field than for the usual semiconductors.[3,14–16] By using the small signal theory, we have also demonstrated that (i) the presence of complex eigenvalues of response matrix, (ii) the negative values taken by the response functions K_v and $K_{\langle s \rangle}$, (iii) the positive overshoot of the corresponding differentials responses $\{\delta v, \delta \widetilde{F}_{\langle s \rangle}\}$, and (iv) the maximum of the real and imaginary parts of the corresponding ac differentials mobility $\{\mu'_v, \mu'_{\langle s \rangle}\}$ are all related to the efficiency of dissipative scattering processes. These results are

connected with the streaming motion of carriers and, in particular, they are evident by means of simplified analytical considerations when the efficiency of dissipative processes prevails on the effects imputable to electric field, by producing a dc NDM for the macroscopic variables v and $F_{\langle s \rangle}$ (i.e., when $X_v(0) < 0$ and $X_{\langle s \rangle}(0) < 0$).

Finally, in Appendixes A–C, we show that for any charge carriers system, where the effective mass is an increasing function (at least linearly) of the microscopic energy, we can always introduce a Lorentz factor for the system.[37] Therefore, as in the monolayer graphene, for very high energies, all carriers travel with a constant group velocity, equally approximately to the saturation maxima velocity. With this constraint, both the electric field and the scattering mechanisms cannot change the modulus of the group velocity, but, as in the monolayer graphene, it can only modify its direction. Therefore, in the case of a single valley model, some analogies between the electron transport in these systems and the electron transport in the monolayer graphene can be considered. In particular, for low electron densities and very high electric fields, due to the delicate equilibrium between the randomization effects and the alignment effects of group velocity, the combined action of band structure and of scattering mechanisms can lead, also in this case, to the onset of a small NDM for the curves of velocity.

We conclude that, under conditions very far from thermal equilibrium, the HD results are found to compare well with those obtained by analogous MC simulations. Therefore, the present HD-MEP method can be fruitfully applied to describe transport properties in graphene with the relevant following advantages: (i) to provide a closed analytical approach and a reduced computational effort with respect to other competitive numerical methods at a kinetic level; (ii) to investigate and classify in a systematic way the behavior of the macroscopic moments in ac and dc dynamic conditions; (iii) to distinguish the different regimes of transport by identifying, from an analysis of collisional frequencies, the dominant scattering mechanisms for a given range of electric field; and (iv) to provide further physical information by allowing the calculation both of entropy and of entropy production associated with the hot carriers of the system.

Lastly, we remark that, for a wider application of the HD-MEP approach, one should consider to further refine the description of the physical system by introducing, for example, the role of the anisotropies in the band structure and electron-phonon coupling elements, the processes for the generation of secondary electrons, and other scattering processes (surface optical-phonon and ionized-impurity scatterings). These implementations can be included in the HD-MEP theory and should be among the topic of future research.

APPENDIX A: CONDUCTIVITY EFFECTIVE MASS

1. Definitions and properties

If we consider an isotropic band structure, with the group velocity $\vec{u}$ and electron momentum $\vec{p} = \hbar\vec{k}$, then we can define[30,31] the isotropic conductivity effective mass $\widetilde{m}(\varepsilon) = \hbar k/u$. In this way, we obtain the differential relation $\widetilde{m}(\varepsilon)\,d\varepsilon = p\,dp$ that we can express in the integral form

$$\int_{E_0}^{\varepsilon} \widetilde{m}(\xi)\,d\xi = \int_{0}^{p} z\,dz = \frac{p^2}{2}, \tag{A1}$$

with E_0 being the energy level corresponding to $\vec{k} = 0$.

By assuming that $\widetilde{m}$ is a nondecreasing function, at least linear[37] in the microscopic energy, then we can write $\widetilde{m} = m[\alpha_0 + 2\alpha_1(\xi - E_0)]$, where for dimensional consistency, m is a mass,[38] α_0 is a dimensionless parameter, and $\alpha_1 \geq 0$ has the dimension of the inverse of an energy. Inserting this expression, for $\widetilde{m}$, into Eq. (A1), by integrating and resolving explicitly this relation, we obtain

$$\alpha_0 + 2\alpha_1(\varepsilon - E_0) = \pm\sqrt{\alpha_0^2 + \frac{2\alpha_1}{m}(\hbar k)^2}. \tag{A2}$$

Thus, in terms of $\vec{k}$ vector, we have the three relations

$$\varepsilon = \left(E_0 - \frac{\alpha_0}{2\alpha_1}\right) \pm \frac{1}{2\alpha_1}\sqrt{\alpha_0^2 + \frac{2\alpha_1}{m}(\hbar k)^2}, \tag{A3}$$

$$\widetilde{m} = m[\alpha_0 + 2\alpha_1(\varepsilon - E_0)], \tag{A4}$$

$$\widetilde{m}u_i = \hbar k_i. \tag{A5}$$

In order to pass from the $\vec{k}$ vector to the group velocity $\vec{u}$, we insert Eq. (A4) in (A5); thus, by squaring Eq. (A5) and using the relations (A2) and (A4), we obtain

$$\frac{1}{(c^\star)^2} = 2\alpha_1 m \geq 0, \tag{A6}$$

$$(\alpha_0 m u)^2 = (\hbar k)^2 \left[1 - \frac{u^2}{c^{\star 2}}\right] \geq 0, \tag{A7}$$

where $c^\star$ is the saturation value of the group velocity. We note that (i) from (A6), when $c^\star \to +\infty \Leftrightarrow \alpha_1 \to 0$. In this case, we do not have any saturation of the group velocity for the system, and the effective mass $\widetilde{m} = \alpha_0 m$ is constant (parabolic-band approximation). Besides, to achieve a finite value of the saturation velocity, the effective mass must be a strictly increasing function of energy (i.e., $\alpha_1 > 0$).

(ii) From (A7), we have $u \leq c^\star$ with $u = c^\star \Leftrightarrow \alpha_0 = 0$. By using Eq. (A7), it is easy to prove the relation

$$\sqrt{\alpha_0^2 + \frac{2\alpha_1}{m}(\hbar k)^2} = |\alpha_0|\Gamma \quad \text{with} \quad \Gamma = \left[1 - \frac{u^2}{c^{\star 2}}\right]^{-\frac{1}{2}}, \qquad \text{(A8)}$$

with Γ being the "Lorentz factor" for the system.

Thus, by using Eqs. (A2) and (A8), we can rewrite the energy (A3) and the effective mass (A4) by means of the Γ factor, ss

$$\varepsilon = \left(E_0 - \frac{\alpha_0}{2\alpha_1}\right) \pm \frac{|\alpha_0|}{2\alpha_1}\Gamma, \quad \widetilde{m} = \pm|\alpha_0|m\Gamma. \qquad \text{(A9)}$$

2. Some significant cases of interest

(I) We assume that $E_0 = \alpha_0/(2\alpha_1)$.

In this case, from (A3), (A4), and (A9), we have

$$\varepsilon = \pm\sqrt{p^2 c^{\star 2} + (\alpha_0 m c^{\star 2})^2} = \pm|\alpha_0|m c^{\star 2}\Gamma, \qquad \text{(A10)}$$

$$\widetilde{m} = \frac{\varepsilon}{c^{\star 2}} = \pm|\alpha_0|m\Gamma. \qquad \text{(A11)}$$

a. Subcase A: Relativistic particle

For $\alpha_0 = 1$ and $c^\star = c$ (where c is the light speed), we obtain the usual relativistic relations

$$\varepsilon = \pm\sqrt{p^2 c^2 + (mc^2)^2} = \pm mc^2\Gamma, \quad \widetilde{m} = \frac{\varepsilon}{c^2} = \pm m\Gamma.$$

b. Subcase B: Monolayer graphene

For $\alpha_0 = 0$ and $c^\star = v_F$, we obtain $E_0 = 0$, with $\Gamma = +\infty$ and the relations[39]

$$\varepsilon = \pm\hbar v_F k, \quad \widetilde{m} = \frac{\varepsilon}{v_F^2}, \quad u_i = v_F n_i. \qquad \text{(A12)}$$

(II) We assume that $E_0 \neq \alpha_0/(2\alpha_1)$.

In this case, we consider the bilayer graphene, the multilayers graphene, and the Kane relation in semiconductors.

c. Subcase C: Bilayer graphene

From (A3), (A4), and (A9), with $\alpha_0/\alpha_1 = \gamma_1 > 0$, $E_0 = \{0, \gamma_1\}$, and $c^\star = v_F$, we determine the simplified expressions[40] for the band structures and the effective mass of the bilayer graphene

$$\varepsilon_{s,\mu} = s\frac{\gamma_1}{2}\left[\mu + \sqrt{1 + \frac{4v_F^2}{\gamma_1^2}(\hbar k)^2}\right] = s\frac{\gamma_1}{2}[\mu + \Gamma], \qquad \text{(A13)}$$

$$\widetilde{m}_s = s\frac{\gamma_1}{2v_F^2}\sqrt{1 + \frac{4v_F^2}{\gamma_1^2}(\hbar k)^2} = s\frac{\gamma_1}{2v_F^2}\Gamma, \qquad \text{(A14)}$$

with $s = \pm$ and $\mu = \pm 1$. In particular, $\varepsilon_{s,-1}$ describes a pair of low-energy bands closer to zero energies and $\varepsilon_{s,+1}$ another pair of high-energy bands repelled away by approximately $\pm\gamma_1$. In each pair, $s = +$ and $s = -$ represent the electron and hole branches, respectively.

The "nonparabolic" low-energy bands, expressed by $\varepsilon_{s,-1}$ interpolates[40] between a linear behavior $\varepsilon_{s,-1} \approx \pm v_F\hbar k$ at very large momenta, and a parabolic quadratic spectrum $\varepsilon_{s,-1} \approx \pm(\hbar k)^2/(2m^\star)$ (with $m^\star = \gamma_1/2v_F^2$) at very small momenta (near the zero energy).

d. Subcase D: ABA-stacked multilayers graphene

The band structure of the multilayer graphene has been observed experimentally[41] and if N is the number of layers, then there are $2N$ energy bands. In particular, in the case of "ABA-stacked multilayers graphene," in a simplified approximation[42] of the tight-binding approach, for N odd, we have the alternation of two linear Dirac bands with $2(N-1)$ nonparabolic bands, while for N even, we have $2N$ nonparabolic bands. For the two linear bands (N odd), we have, as in "Subcase B," $\varepsilon = \pm\hbar v_F k$ and $\widetilde{m} = \varepsilon/v_F^2$. The remaining nonparabolic bands (for both N odd and N even) can be determined from the relations (A3), (A4), and (A9) by assuming $c^\star = v_F$, $\alpha_0/\alpha_1 = \gamma_{1,n} = \gamma_1 \Upsilon_n > 0$, and $E_0 = \{0, \gamma_{1,n}\}$, with

$$\Upsilon_n = 2\cos\left(\frac{\pi n}{N+1}\right), \quad n = 1, 2, \ldots [N/2],$$

where $[N/2]$ is the greatest integer $\leq N/2$.

In this case, we obtain a generalization of (A13)–(A14)

$$\varepsilon_{s,\mu}^n = s\frac{\gamma_{1,n}}{2}\left[\mu + \sqrt{1 + \frac{4v_F^2}{\gamma_{1,n}^2}(\hbar k)^2}\right] = s\frac{\gamma_{1,n}}{2}[\mu + \Gamma], \qquad \text{(A15)}$$

$$\widetilde{m}_s^n = s\frac{\gamma_{1,n}}{2v_F^2}\sqrt{1 + \frac{4v_F^2}{\gamma_{1,n}^2}(\hbar k)^2} = s\frac{\gamma_{1,n}}{2v_F^2}\Gamma, \qquad \text{(A16)}$$

with $s = \pm, \mu = \pm 1$, and $n = 1, \ldots, [N/2]$.

Thus, for "ABA-stacked trilayer graphene" $N = 3$, we have six energy bands[43,44] with the energy spectrum, that is, the superposition of two linear Dirac bands [see Eqs. (A12)], as in the monolayer graphene, and four nonparabolic bands, as in the bilayer graphene, except that the term γ_1 will appear with a factor of $\sqrt{2}$ (i.e., $\gamma_{1,1} = \sqrt{2}\gamma_1$, $\varepsilon_{s,\mu}^1 = s(\gamma_1/\sqrt{2})[\mu + \Gamma]$, and $\widetilde{m}_s^1 = s\gamma_1/(\sqrt{2}v_F^2)\Gamma)$.

Analogously, for "ABA-stacked four-layer graphene" $N = 4$, we have eight nonparabolic bands with different values of effective masses,[44] obtained by inserting in (A15) and (A16) $\gamma_{1,1} = (\sqrt{5}+1)$ $\gamma_1/2$ and $\gamma_{1,2} = (\sqrt{5}-1)\gamma_1/2$.

Finally, for $N = 5$, we have the "ABA-stacked five-layer graphene" and, therefore, still an alternation of two linear Dirac bands [Eqs. (A12)], with eight nonparabolic bands and different effective masses[44] obtained by introducing the values $\gamma_{1,1} = \sqrt{3}\gamma_1$ and $\gamma_{1,2} = \gamma_1$ in (A15) and (A16).

It is clear that the band structure becomes more and more complex with increasing the number N of layers, but in the framework of these approximations,[42] both the energy and the effective mass can be determined using, in a recursive way, the relations (A12), (A15), and (A16).

e. Subcase E: Kane relation in semiconductors

In this case, $\alpha_0 = 1$, α_1 is the nonparabolicity factor, $E_0 = E_c$ and m are, respectively, the energy and the effective mass associated with the bottom edge of the conduction band. Thus, by using (A3), (A4), and (A9), we obtain

$$\varepsilon - E_c = \frac{1}{2\alpha_1}\left\{-1 + \sqrt{1 + \frac{2\alpha_1}{m}(\hbar k)^2}\right\} = mc^{\star 2}(\Gamma - 1),$$

$$\widetilde{m} = m[1 + 2\alpha_1(\varepsilon - E_c)] = m\Gamma,$$

where $c^{\star 2} = (2\alpha_1 m)^{-1}$. Also in this case, the nonparabolic energy interpolates between quadratic forms $\varepsilon - E_c \approx (\hbar k)^2/(2m)$ near the zero energy (i.e., $\varepsilon = E_c$), and a linear behavior $\varepsilon - E_c \approx c^\star \hbar k$ at very high momenta.

Therefore, for any physical system in which the conductivity effective mass is a strictly increasing function, at least linear[37] in the microscopic energy, we have (i) a saturation velocity for the group velocity and we can express both the band structure and the effective mass in terms of a "Lorentz factor" Γ for the system.

(ii) By knowing the three parameters $\widetilde{\alpha}_0 = m\alpha_0$, $\widetilde{\alpha}_1 = m\alpha_1$, and E_0, we explicitly determine both the band structure of the physical system considered and the saturation velocity for the group velocity. In particular, $\widetilde{\alpha}_0$ and $\widetilde{\alpha}_1$ can be obtained by means of experimental measurements of the carriers' effective mass.[44,45]

APPENDIX B: BAND STRUCTURE, ELECTRIC FIELD, AND DISSIPATIONS

1. Linear band structure

In the case of the monolayer graphene, due to a linear band structure, the carriers must travel keeping the modulus of the group velocity constant. Thus, if we decompose the group velocity and the momentum into their parallel and perpendicular parts to the applied field **E**, we have $|\mathbf{u}| = v_F = \sqrt{(\mathbf{u}^\parallel)^2 + (\mathbf{u}^\perp)^2}$ with $\mathbf{u}^\perp = \hbar \mathbf{k}^\perp/\widetilde{m}(\varepsilon)$ and $\mathbf{u}^\parallel = \hbar \mathbf{k}^\parallel/\widetilde{m}(\varepsilon)$.

It is easy to prove that the electrons moving in the direction of an increasing electric field will have the parallel component $\mathbf{u}^\parallel$ increasing at the expense of its perpendicular part $\mathbf{u}^\perp$. Indeed, in correspondence of an increase $\delta\mathbf{E}$ of the electric field in the direction of its application, the energy $\varepsilon(k)$ increases, the effective mass $\widetilde{m}(\varepsilon)$ increases, and the electron momentum $\hbar\mathbf{k}$ increases only in the direction parallel to $\delta\mathbf{E}$ (while it remains constant in the perpendicular direction); this leads to a decrease of the component $\mathbf{u}^\perp$ and, for the constrain $|\mathbf{u}| = v_F$, to an increase of the parallel component $\mathbf{u}^\parallel$. Therefore, an increasing electric field tends to align the group velocity (by keeping its modulus constant) in the direction of the applied field. Vice versa, the scattering mechanisms dissipate energy and redistribute momentum in different directions, and, consequently, they randomize the group velocity in the phase space, leaving its modulus unchanged.

Thus, the macroscopic quantities v_i and $\widetilde{F}_{\langle i_1 \ldots i_s\rangle}$ can be evaluated as an ensemble average of the versors n_i, with

$$v_i = \frac{v_F}{n}\int n_i \mathscr{F} d\vec{k}, \quad \widetilde{F}_{\langle i_1 \ldots i_s\rangle} = \frac{v_F^s}{n}\int n_{\langle i_1} \ldots n_{i_s\rangle} \mathscr{F} d\vec{k}. \quad \text{(B1)}$$

Therefore, if the aligning effects prevail on the randomization processes, we have an anisotropy of the distribution function in the direction of the applied field, and the moments $\{v_i, \widetilde{F}_{\langle i_1 \ldots i_s\rangle}\}$ increase. Vice versa, if the scattering mechanisms prevail with respect to the electric field effects, then the randomization processes tend to isotropize the distribution function, and the moments decrease. In order to verify whether the randomization processes can produce strong dissipative phenomena on the macroscopic variables (B1), we consider the effects imputable to the choice of a different acoustic deformation potential D_{ac} for the elastic intravalley transitions, leaving the other scattering parameters unchanged. We remark that the intravalley acoustic scattering can only randomize both the momentum and the group velocity of the electrons. In this case, the scattering events, being elastic, do not change the $|k|$ of electrons (although $|k|$ is different for the single carriers), while $|u| = v_f$ is always constant (regardless of the scattering processes) and the same for all electrons, due to the linear band.

In particular, we use a larger deformation potential $D_{ac} = 16.5 \cdot \sqrt{8}\,\text{eV}$, equivalent to that adopted by Shishir[46] and co-workers in Ref. 23, and in Fig. 12, we report the new HD numerical results for both the collisional frequencies and the average velocity in correspondence of different electron densities. In this case, we obtain two distinct total average collisional frequencies, respectively, for the velocity v $(C^{op} + C^{iv} + C_1^{EL})$ and for the remaining deviatoric moments $\widetilde{F}_{\langle s\rangle}$ $(C^{op} + C^{iv} + C_s^{EL})$ with $s > 1$. Obviously, the inelastic collisional frequencies $\{C^{op}, C^{iv}\}$, reported in Fig. 12, remained unchanged with respect to the previously examined case (see Fig. 1); while on the contrary, the elastic collisional frequencies C_1^{EL} and C_s^{EL} are no more negligible by assuming, in this case, a dominant role for all energy ranges. Figure 12 reports the collision frequencies $\{C^\eta, C_1^{El}, C_s^{El}\}$ [Eqs. (30) and (32)] as functions of average electron energy eW, and HD stationary numerical results for the velocity as function of electric field E, for different electron densities. Thus, if on the one hand, the linear dispersion $\varepsilon(k)$ forces the electrons to travel with a group velocity of constant modulus then, on the other hand, the scattering mechanisms, by producing a randomization of the group velocity, tend to isotropize the distribution function and consequently all moments (B1) strongly decrease. Analogously, both Figs. 1 and 12 show that, for very low electric fields, the collisional frequencies strongly depend on the electron density. Consequently, the behavior of the NDM will depend strongly on the electron density.
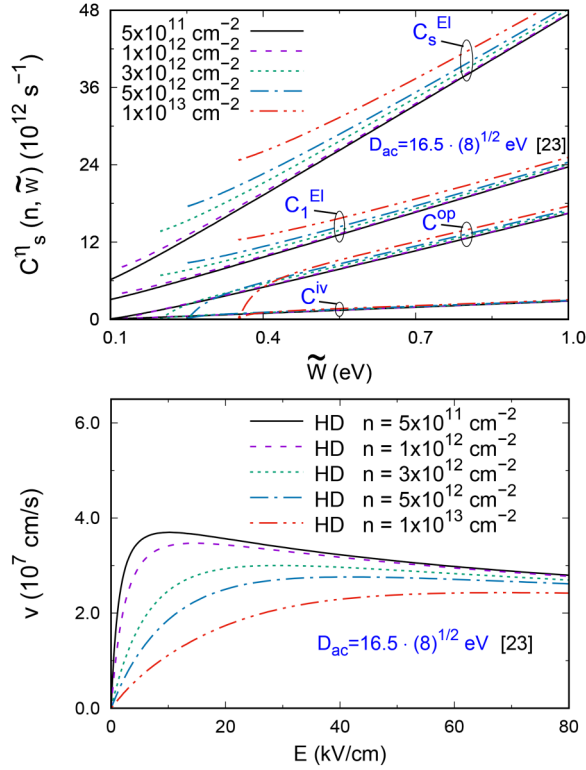
FIG. 12. Collision frequencies $\{C^\eta, C_1^{El}, C_s^{El}\}$ [Eqs. (30) and (32)] vs average electron energy $\widetilde{W}$, and HD stationary numerical results for the velocity vs electric field E, for different electron densities. In this case, for the inelastic transitions $\eta = \{op, iv\}$, we have taken the same effective parameters used by Borysenko and co-workers[19,20] in Eqs. (13), while for the elastic acoustic intravalley transitions, we have adopted a different deformation potential D_{ac} used by Shishir and Ferry in Ref. 23.

2. Nonparabolic band structure

In this case, due to the band structure, the carriers do not travel with a constant velocity and, for $u(k) \ll c^*$, the electric field and the dissipative processes produce reciprocal variations both of

the modulus and the direction of the group velocity. Thus, the average velocity and all deviatoric moments will be expressed as a statistical average on both the modulus $u(k)$ and the versor n_i, where $v_i = 1/n \int u(k) n_i \mathscr{F} \, d\vec{k}$ and $\widetilde{F}_{\langle i_1 \dots i_s \rangle} = 1/n \int [u(k)]^s n_{\langle i_1} \dots n_{i_s \rangle} \mathscr{F} \, d\vec{k}$.

However, for very large momenta, the band structure exhibits a linear dispersion and the carriers should travel, approximatively, with a constant group velocity coinciding with the saturation velocity (i.e., $u \approx c^*$). Consequently, in this case, both the electric field and the scattering mechanisms cannot change the modulus of the group velocity but can only modify its direction and, as in the monolayer graphene, v_i and $\widetilde{F}_{\langle i_1 \dots i_s \rangle}$ will be expressed only as an ensemble average of the versors n_i.

Consequently, in the case of a single effective valley with a nonparabolic band structure when, for very high fields, it can be considered approximately linear, the prevalence of effects due to randomization of group velocity can lead to small negative differential mobility both for the values of average velocity v_i and for the values of deviatoric moments $\widetilde{F}_{\langle i_1 \dots i_s \rangle}$.

APPENDIX C: SMALL-SIGNAL ANALYSIS

By considering the time evolution of a small perturbation around the steady state of the moments $\widetilde{F}_\alpha$, the system of Eq. (40) is expressed in terms of the $M + 1$ quantities $\delta\widetilde{F}_\alpha(t) = \left\{ \delta\widetilde{W}, \delta v, \delta\widetilde{F}_{\langle s \rangle} \right\}^T$ (with $s = 2, \dots, M$). For the component of the "perturbing forces," we have $\Gamma_\alpha^{(E)} = K_\alpha(0) = \{\Gamma_{\widetilde{W}}^{(E)}, \Gamma_v^{(E)}, \Gamma_{\langle s \rangle}^{(E)}\}^T$, where

$$\Gamma_{\widetilde{W}}^{(E)} = K_{\widetilde{w}}(0) = v, \tag{C1}$$

$$\Gamma_v^{(E)} = K_v(0) = \frac{1}{2}\left\langle \frac{1}{\widetilde{m}} \right\rangle - \widetilde{F}_{(-1)|\langle 2 \rangle}, \tag{C2}$$

$$\Gamma_{\langle s \rangle}^{(E)} = K_{\langle s \rangle}(0) = s\left[\frac{v_F^2}{4}\widetilde{F}_{(-1)|\langle s-1 \rangle} - \widetilde{F}_{(-1)|\langle s+1 \rangle}\right] \tag{C3}$$

for $s = 2, \dots, M$.

Analogously, for the asymmetric $(M + 1) \times (M + 1)$ response matrix $\Gamma_{\alpha\beta}$, we have

$$
\Gamma_{\alpha\beta} =
\begin{bmatrix}
\Gamma_w^{(0)} & -eE & 0 & 0 & 0 & 0 & \cdots & 0 & 0 & 0 \\
\Gamma_w^{(1)} & \mathscr{C}_1 & \chi eE & 0 & 0 & 0 & \cdots & 0 & 0 & 0 \\
\Gamma_w^{(2)} & -\frac{\chi v_F^2}{2}eE & \mathscr{C}_2 & 2\chi eE & 0 & 0 & \cdots & 0 & 0 & 0 \\
\Gamma_w^{(3)} & 0 & -\frac{3\chi v_F^2}{4}eE & \mathscr{C}_2 & 3\chi eE & 0 & \cdots & 0 & 0 & 0 \\
\vdots & \vdots & \vdots & \vdots & \vdots & \vdots & \cdots & \vdots & \vdots & \vdots \\
\Gamma_w^{(M-1)} & 0 & 0 & 0 & 0 & 0 & \cdots & -\frac{(M-1)\chi v_F^2}{4}eE & \mathscr{C}_2 & (M-1)\chi eE \\
\Gamma_w^{(M)} & 0 & 0 & 0 & 0 & 0 & \cdots & 0 & -\frac{M\chi v_F^2}{4}eE & \mathscr{C}_2
\end{bmatrix}
$$

where $\mathscr{C}_1 = -[\sum_\eta C^\eta + C_1^{El}]$, $\mathscr{C}_2 = -[\sum_\eta C^\eta + C_2^{El}]$, the function χ is expressed by Eq. $(25)_2$ and all the elements $\Gamma_w^{(s)}$ of the first column can be expressed by introducing the "chord mobility generalized moments" $\mu_w = \widetilde{W}/E$, $\mu_v = v/E$, $\mu_{\langle s\rangle} = \widetilde{F}_{\langle s\rangle}/E$ and the "differential mobility generalized moments" $\mu_w' = d\widetilde{W}/dE$, $\mu_v' = dv/dE$, and $\mu_{\langle s\rangle}' = d\widetilde{F}_{\langle s\rangle}/dE$, with the conditions $\mu_{\langle M+1\rangle} = \mu_{\langle M+1\rangle}' = 0$. Thus, we obtain

$$\Gamma_w^{(0)} = eE\frac{\mu_v' + \mu_v}{\mu_w'},$$

$$\Gamma_w^{(1)} = -eE\chi\frac{\mu_{\langle 2\rangle}' + \mu_{\langle 2\rangle}}{\mu_w'} - \mathscr{C}_1\frac{\mu_v'}{\mu_w'} + \frac{ev_F^2}{2\mu_w'}\widetilde{F}_{(-1)},$$

$$\Gamma_w^{(2)} = 2eE\chi\left[\frac{v_F^2}{4}\frac{\mu_v' + \mu_v}{\mu_w'} - \frac{\mu_{\langle 3\rangle}' + \mu_{\langle 3\rangle}}{\mu_w'}\right] - \mathscr{C}_2\frac{\mu_{\langle 2\rangle}'}{\mu_w'},$$

$$\vdots$$

$$\Gamma_w^{(p)} = peE\chi\left[\frac{v_F^2}{4}\frac{\mu_{\langle p-1\rangle}' + \mu_{\langle p-1\rangle}}{\mu_w'} - \frac{\mu_{\langle p+1\rangle}' + \mu_{\langle p+1\rangle}}{\mu_w'}\right]$$
$$- \mathscr{C}_2\frac{\mu_{\langle p\rangle}'}{\mu_w'} \quad \text{with} \quad p = 3, \ldots, M,$$

It is worth noting that, if we know explicitly the response matrix $\Gamma_{\alpha\beta}$ and the vector $\Gamma_\alpha^{(E)}$, then we can construct an "algebraic" formulation of theory.

Thus, for a "steplike switching perturbation," with an integration of Eq. (41), we obtain the following algebraic expression for the "differential response":

$$\delta\widetilde{F}_\alpha(t)/\delta E = -e\Gamma_{\alpha\beta}^{-1}[K_\beta(t) - \Gamma_\beta^{(E)}]. \tag{C4}$$

Analogously, for an "harmonic perturbation," the real and imaginary parts of $\mu_\alpha'(\omega) = X_\alpha(\omega) + iY_\alpha(\omega)$ can be evaluated separately in the algebraic form

$$X_\alpha(\omega) = e\Gamma_{\alpha\beta}\left[\Gamma_{\beta\gamma}^2 + \omega^2\delta_{\beta\gamma}\right]^{-1}\Gamma_\gamma^{(E)}, \tag{C5}$$

$$Y_\alpha(\omega) = e\omega\left[\Gamma_{\alpha\gamma}^2 + \omega^2\delta_{\alpha\gamma}\right]^{-1}\Gamma_\gamma^{(E)}, \tag{C6}$$

with the condition

$$X_\alpha(0) = [d\widetilde{F}_\alpha/dE]_{dc}. \tag{C7}$$

where $[d\widetilde{F}_\alpha/dE]_{dc}$ is the "dc generalized differential mobility" of the corresponding moments $\widetilde{F}_\alpha$. We remark that, also in the limiting forms ($\omega \to 0$ and/or $\omega \to \infty$), some analytical algebraic expressions can be explicitly determined. Thus, in the "low frequency limit," we obtain

$$X_\alpha \approx X_\alpha(0) + \frac{1}{2}\left[\frac{d^2X_\alpha}{d\omega^2}\right]_0\omega^2, \quad Y_\alpha \approx \left[\frac{dY_\alpha}{d\omega}\right]_0\omega, \tag{C8}$$

with the general relations

$$X_\alpha(0) = -e\int_0^\infty K_\alpha(s)\,ds = e\Gamma_{\alpha\beta}^{-1}\Gamma_\beta^{(E)}, \tag{C9}$$

$$\left[\frac{dY_\alpha}{d\omega}\right]_0 = e\int_0^\infty sK_\alpha(s)\,ds = e\left(\Gamma_{\alpha\beta}^{-1}\right)^2\Gamma_\beta^{(E)}, \tag{C10}$$

$$\left[\frac{d^2X_\alpha}{d\omega^2}\right]_0 = e\int_0^\infty s^2K_\alpha(s)ds = -2e\left(\Gamma_{\alpha\beta}^{-1}\right)^3\Gamma_\beta^{(E)}. \tag{C11}$$

Analogously, in the "high frequency limit," we have

$$X_\alpha(\omega) \approx \frac{e}{\omega^2}\left[\frac{dK_\alpha}{dt}\right]_{0^+}, \quad Y_\alpha(\omega) \approx \frac{e}{\omega}K_\alpha(0), \tag{C12}$$

with the general relations

$$\int_0^\infty X_\alpha d\omega = -\frac{\pi}{2}eK_\alpha(0), \quad \int_0^\infty \frac{1}{\omega}Y_\alpha d\omega = -\frac{\pi}{2}X_\alpha(0). \tag{C13}$$

REFERENCES

[1] E. T. Jaynes, Phys. Rev. **106**, 620 (1957); **108**, 171 (1957).

[2] Maximum Entropy and Bayesian Methods, edited by J. Skilling (Kluwer Academic Publishers, 2004).

[3] M. Trovato and L. Reggiani, Riv. Nuovo Cimento **35**, 99–266 (2012).

[4] I. Müller and T. Ruggeri, Rational Extended Thermodynamics (Springer-Verlag, New York, 1998), Vol. 37.

[5] T. Ruggeri and M. Sugiyama, Rational Extended Thermodynamics Beyond the Monatomic Gas (Springer, 2015).

[6] D. Jou, G. Lebon, and J. Casas-Vazquez, Extended Irreversible Thermodynamics (Springer, 2010).

[7] M. Trovato and L. Reggiani, Phys. Rev. E **81**, 021119 (2010).

[8] M. Trovato and L. Reggiani, Phys. Rev. E **84**, 061147 (2011).

[9] M. Trovato and L. Reggiani, Phys. Rev. Lett. **110**, 020404 (2013).

[10] M. Trovato and P. Falsaperla, Phys. Rev. B **57**, 4456 (1998).

[11] M. Trovato and L. Reggiani, J. Appl. Phys. **85**, 4050 (1999).

[12] M. Trovato, P. Falsaperla, and L. Reggiani, J. Appl. Phys. **86**, 5906 (1999).

[13] M. Trovato and L. Reggiani, Phys. Rev. B **61**, 16667 (2000).

[14] M. Trovato and L. Reggiani, Phys. Rev. B **73**, 245209 (2006).

[15] R. Rengel, J. Iglesias, E. Pascual, and M. Martin, J. Appl. Phys. **121**, 185705 (2017).

[16] L. Reggiani, E. Starikov, P. Shiktorov, V. Gruzinskis, and L. Varani, Semicond. Sci. Technol. **12**, 141 (1997).

[17] M. Fischetti, J. Kim, S. Narayanan, Z. Ong, C. Sachs, D. Ferry, and S. Aboud, J. Phys. Condens. Matter **25**, 473202 (2013).

[18] S. Piscanec, M. Lazzeri, F. Mauri, A. C. Ferrari, and J. Robertson, Phys. Rev. Lett. **93**, 185503 (2004); **95**, 236802 (2005).

[19]K. M. Borysenko, J. T. Mullen, E. A. Barry, S. Paul, Y. G. Semenov, J. M. Zavada, M. B. Nardelli, and K. W. Kim, Phys. Rev. B **81**, 121412(R) (2010).

[20]R. Rengel, C. Couso, and M. Martin, in *Spanish Conference on Electron Devices (CDE)* (IEEE, 2013), Vol. 175; R. Rengel, E. Pascual, and M. Martin, Appl. Phys. Lett. **104**, 233107 (2014).

[21]E. H. Hwang and S. D. Sarma, Phys. Rev. B **77**, 115449 (2008).

[22]M. Lazzeri, C. Attaccalite, L. Wirtz, and F. Mauri, Phys. Rev. B **78**, 081406 (2008).

[23]R. S. Shishir and D. K. Ferry, J. Phys. Condens. Matter **21**, 232204 (2009); **21**, 344201 (2009).

[24]By introducing the same scattering parameters for both TO and LO transitions, the angular dependence disappears in the sum $Q_{TO} + Q_{LO}$. This sum can be described with a single optical mode using the simplified term (8).

[25]For example, Piscanec and co-workers (see Refs. 18 and 22) assume that the $K-K'$ inelastic intervalley processes are assisted, near the K-line, only by means of optical A'_1 phonons. In this case, the GW-corrected DFT[22] was used to extract different scattering parameters. However, these values have been determined, in the context of Kohn anomalies, only for transitions between symmetry points and they cannot be easily compared with the scattering parameters that appear be averaged over entire BZ,[17,19] when the interactions with the entire phonon system is taken into account.

[26]In Refs. 19 and 20, the authors, to fit their DFT calculations, appear to consider the expression employed in Ref. 21, multiplying Eq. (11) for another angular factor $(1 - \cos\theta)$. In this way, an additional factor $1/2$ in their final calculations is introduced. Consequently, to compare the HD simulations in the same conditions of MC calculations, by using the scattering rate (12), we must assume that $D_{ac} = D_{ac}^{MC}/\sqrt{2}$.

[27]X. Li, E. A. Barry, J. M. Zavada, M. Buongiorno Nardelli, and K. W. Kim, Appl. Phys. Lett. **97**, 232105 (2010).

[28]X. Li, K. M. Borysenko, M. Buongiorno Nardelli, and K. W. Kim, Phys. Rev. B **84**, 195453 (2011).

[29]The more general choice of kinetic fields is given by $\psi_A = \{\varepsilon^r u_{\langle i_1 \ldots i_s\rangle}\}$ and by the corresponding macroscopic variables $F_{(r)|\langle i_1 \ldots i_s\rangle} = \int \varepsilon^r u_{\langle i_1} \ldots u_{i_s\rangle} \mathscr{F} \, d\vec{k}$, with $r = 0, 1, \ldots, N$ and $s = 0, 1, \ldots, M$. Indeed, with this choice we can include, as particular case, the set of kinetic fields used in this paper and any other set of kinetic field, built by using, for example, polynomial expressions in the microscopic momentum $p_i = \hbar k_i$. Indeed, due to the linear band structure, the macroscopic variable $P_i = \int p_i \mathscr{F} \, d\vec{k}$ is proportional to the energy flux, while for more general moments, $P_{\langle i_1 \ldots i_s\rangle} = \int p_{\langle i_1} \ldots p_{i_s\rangle} \mathscr{F} \, d\vec{k}$, we obtain $P_{\langle i_1 \ldots i_s\rangle} = F_{(s)|\langle i_1 \ldots i_s\rangle}/v_F^{2s}$. However, it is possible to show that by using the set (14), we obtain the faster convergent HD system, in the framework of moments method.

[30]C. Jacoboni and P. Lugli, *The Monte Carlo Method for Semiconductor Device Simulation* (Springer-Verlag, 1989).

[31]V. Ariel, e-print arXiv:1205.3995v1 (2012); V. Ariel and A. Natan, e-print arXiv:1206.6100v1 (2012).

[32]In correspondence with the densities $n = 3 \cdot 10^{12}$ cm^{-2}; $n = 5 \cdot 10^{12}$ cm^{-2}; and $n = 10^{13}$ cm^{-2}, the collision frequencies C^η are strongly increasing, respectively, in the energy ranges [0.2, 0.3] (eV); [0.25, 0.34] (eV); [0.35, 0.44] (eV) (or, equivalently, in the ranges of electric field [0, 8] (kV/cm); [0, 10] (kV/cm); and [0, 20] (kV/cm)).

[33]In the limit case in which $\widetilde{F}_{(-1)|\langle 2\rangle} \to 0$, Eqs. (33) and (39) for $\widetilde{W}$ and v are completely decoupled from Eqs. (35). Thus, we obtain the final convergence of $\widetilde{W}$ and v only with $M = 1$.

[34]Also the remaining deviatoric moments $F_{\langle s\rangle}$ converge toward the same final value only for large values of M.

[35]M. Nedjalkov, H. Kosina, and S. Selberherr, in *Proceedings of the International Conference on Simulation of Semiconductor Processes and Devices SISPAD'99*, edited by K. Taniguchi and N. Nakayama (Business Center for Academy Society Japan, Kyoto, 1999), p. 155.

[36]If $X_v(0)$ is strictly negative and $K_v(0) > 0$, then from Eq. (C13)$_1$ also $X_v(\omega)$ should increase to compensate and pass, through a zero value, from negative to positive values.

[37]If $\widetilde{m}$ is expressed by means of a nonlinear function of ε, then (A4) can be considered only as a its first linear approximation $\widetilde{m}^{(1)}$. Therefore, using Eq. (A1), we will determine a more complicated expression for the energy with respect to a nonparabolic band structure (A3). However, by assuming that $\widetilde{m}$ is an increasing function of the energy with $\widetilde{m}(\varepsilon) \geq m^{(1)}(\varepsilon)$, we obtain still a saturation velocity for the system, where $|\vec{u}| = \hbar|\vec{k}|/\widetilde{m} \leq \hbar|\vec{k}|/\widetilde{m}^{(1)} \leq c^\star$.

[38]We remark that m is introduced only for dimensional reasons. Indeed, in Eq. (A2), $\widetilde{m}$ can be redefined only in terms of the new quantities $\widetilde{\alpha}_0 = m\alpha_0$ and $\widetilde{\alpha}_1 = m\alpha_1$ that are the only two experimental parameters that allow us to determine explicitly the conductivity effective mass.

[39]If $\alpha_0 \to 0$, then $u \to c^\star$ and $\Gamma \to +\infty$, but the quantity $|\alpha_0|\Gamma$ tends always to finite value.

[40]E. McCann and V. I. Falko, Phy. Rev. Lett. **96**, 086805 (2006); E. McCann, D. S. L. Abergel, and V. I. Falko, Eur. Phys. J. Special Top. **148**, 91 (2007); M. Koshino, New J. Phys. **11**, 095010 (2009).

[41]T. Ohta, A. Bostwick, J. L. McChesney, T. Seyller, K. Horn, E. Rotenberg, Phys. Rev. Lett. **98**, 206802 (2007).

[42]In a first approximation, we can neglect all interactions except those between the nearest-neighbor atoms in the same layer and between A-type atoms adjacent layer which are on the top of each other.

[43]F. Guinea, A. H. Castro Neto, and N. M. R. Peres, Phys. Rev. B **73**, 245426 (2006); M. Koshino and E. McCann, Phy. Rev. B **79**, 125443 (2009).

[44]R. S. Thompson, Y. C. Chang, and J. G. Lu, Eur. Phys. J. B **85**, 13 (2012).

[45]A. Gruneis, C. Attaccalite, L. Wirtz, H. Shiozawa, R. Saito, T. Pichler, and A. Rubio, Phys. Rev. B **78**, 205425 (2008).

[46]Shishir and co-workers[23,46] have employed an expression similar to Eq. (22) but with a factor of eight in the numerator and with an acoustic deformation potential $D_{ac}^{MC} = 16.5$ eV. Therefore, in order to consider the same expression in the present HD model, we must assume in Eq. (22) $D_{ac} = 16.5 \cdot \sqrt{8}$ eV. Besides, they seem to ignore the inelastic intervalley (iv) transitions, by using the coupling constant $D_{op}^{MC} = 10^9$ eV/cm (as in the present paper) but with a smaller optical phonon energy of $\omega_{op} = 150$ meV.